

Flares In Long And Short Gamma Ray Bursts

Shlomo Dado¹ and Arnon Dar²

ABSTRACT

The many similarities between the prompt emission pulses in gamma ray bursts (GRBs) and X-ray flares during the fast decay and afterglow phases of GRBs suggest a common origin. In the cannonball (CB) model of GRBs, this common origin is mass accretion episodes of fall-back matter on a newly born compact object. The prompt emission pulses are produced by a bipolar jet of highly relativistic plasmoids (CBs) ejected in the early, major episodes of mass accretion. As the accretion material is consumed, one may expect the engine's activity to weaken. X-ray flares ending the prompt emission and during the afterglow phase are produced in such delayed episodes of mass accretion. The common engine, environment and radiation mechanisms (inverse Compton scattering and synchrotron radiation) produce their observed similarities. Flares in both long GRBs and short hard gamma ray bursts (SHBs) can also be produced by bipolar ejections of CBs following a phase transition in compact objects due to loss of angular momentum and/or cooling. Optical flares, however, are mostly produced in collisions of CBs with massive stellar winds/ejecta or with density bumps along their path. In this paper we show that the master formulae of the CB model of GRBs and SHBs, which reproduce very well their prompt emission pulses and their smooth afterglows, seem to reproduce also very well the lightcurves and spectral evolution of the prominent X-ray and optical flares that are well sampled.

Subject headings: gamma rays: bursts

1. Introduction

A flaring activity during the afterglow (AG) phase of a gamma ray burst (GRB) was first observed in the late-time AG of GRB 970508 with the Narrow Field Instrument (NFI)

¹dado@phep3.technion.ac.il

Physics Department, Technion, Haifa 32000, Israel

²arnon@physics.technion.ac.il

Physics Department, Technion, Haifa 32000, Israel

aboard the BeppoSAX satellite in the X-ray band (Piro et al. 1998), and with ground based telescopes in the optical band (Pian et al. 1998; Galama et al. 1998a). It was interpreted in the framework of the fireball (FB) model of GRBs as a delayed burst from the central GRB engine (Piro et al. 1998). Alternatively, in the cannonball (CB) model of GRBs it was interpreted as a synchrotron radiation (SR) flare from an encounter of the highly relativistic jetted ejecta from an underlying supernova (SN) explosion with a density jump in the interstellar medium (Dado et al. 2002, 2004). Late-time flares were later discovered in the broadband AG of several other GRBs that were localized by the BeppoSAX satellite, most notably in GRB 000301C at $t \sim 4$ days after burst (Berger et al. 2000; Sagar et al. 2000) where the flare was attributed to gravitational microlensing (Garnavich et al. 2000) and in GRB 030329 (Lipkin et al. 2004) where the flare was interpreted in the framework of the FB model as due to ‘refreshed shocks’ generated by a late activity of the central engine (Granot et al. 2003). In the CB model, however, these flares were well reproduced by the emission of SR from encounters of the jetted ejecta from an underlying SN explosion in a star formation region with density jumps within or at the border of a super bubble created by the star formation region (Dado et al. 2002, 2004).

Early-time X-ray flares ending the prompt emission phase were also detected by the wide field camera (WFC) aboard BeppoSAX in a few GRBs such as GRB 011121. In the FB model they were attributed to the onset of the external shock in the circumburst material. In the CB model they were interpreted as being due to the last episodes of bipolar CB ejections from a shutting off central engine. Shortly after the launch of the Swift satellite in November 2004, data collected with its X-ray telescope (XRT) showed that X-ray flares are quite common in all the phases of the emission from GRBs. In more than 50% of the GRBs observed with the Swift X-ray telescope (XRT), flares were observed at the end of the prompt emission and/or the early AG phase (Burrows et al. 2005, 2007; Falcone et al. 2007). In some cases X-ray flares were observed also at very late times, of the order of several days after the prompt emission. Although the information on flares is much more sketchy compared to that on the prompt gamma ray pulses, their spectral and temporal behaviours show clearly that the X-ray flares during the prompt γ -ray emission follow the pattern of the γ -ray pulses, suggesting they are the low energy part of these pulses. The X-ray flares ending the prompt emission and those superimposed on the early-time afterglow have a fast spectral evolution. Their peak intensities decrease with time, and their spectral and temporal behaviours are similar to those of the prompt X/ γ -ray pulses, except that they are progressively softer and last longer. In most cases their γ -ray emission probably is below the detection sensitivity of the Swift broad alert telescope (BAT). In some cases their fluence in the XRT band exceeded that of the prompt emission in the BAT 15-150 keV band (Chincarini et al. 2008a,b).

Late-time ($t \gtrsim 10^4$ s) X-ray flares, however, seem to exhibit temporal and spectral behaviours that are different from those of most of the early-time flares. Their power-law decline is more moderate, they are "achromatic" with a power-law spectrum almost identical to that of the late-time AG, and they show very little spectral evolution (see, e.g., the late time broad band flares in GRBs 060614 (Mangano et al. 2007) and 081028 (Margutti et al. 2009), and the hardness ratio during late time flares in Swift GRBs reported in the Swift-XRT lightcurve repository, Evans et al. (2009)).

Flares in the X-ray lightcurve of Swift GRBs were studied phenomenologically by various observer groups (Burrows et al. 2005, 2007; Kocevski and Butler 2007; Butler and Kocevski 2007; Falcone et al. 2007; Chincarini et al. 2007a,b, 2008a,b). Modifications of previously suggested models and new theoretical models were proposed and discussed by several authors (Proga et al. 2005; King et al. 2005; Dai et al. 2006; Fan et al. 2006; Perna et al. 2006), but none of these proposed models was shown to actually derive the observed lightcurves and spectral evolution of either early-time or late-time flares from underlying physical assumptions.

Flares are a natural consequence of the cannonball (CB) model of GRBs, which was motivated by a GRB-microquasar analogy (Dado et al. 2002; Dar and De Rújula 2004). In the CB model, *long-duration* GRBs and their AGs are produced by bipolar jets of highly relativistic plasmoids of ordinary matter ejected in accretion episodes on the newly formed compact stellar object (Shaviv and Dar 1995; Dar 1998) in core-collapse supernova (SN) explosions (Dar et al. 1992; Dar and Plaga 1999). It is hypothesized that an accretion disk or a torus is produced around the newly formed compact object, either by stellar material originally close to the surface of the imploding core and left behind by the explosion-generating outgoing shock, or by more distant stellar matter falling back after its passage (De Rújula 1987). As observed in microquasars (Mirabel and Rodriguez 1999), each time part of the accretion disk falls abruptly onto the compact object, two jets of cannonballs (CBs) made of *ordinary-matter plasma* are emitted with large bulk-motion Lorentz factors in opposite directions along the rotation axis, wherefrom matter has already fallen back onto the compact object due to lack of rotational support. The entire radiation emitted from a GRB is produced by the interaction of the jet of CBs with the environment along its path, as illustrated in Fig. 1. The prompt γ -ray and X-ray emission is dominated by inverse Compton scattering (ICS) of photons of the SN light filling the cavity produced by the pre-supernova wind/ejecta blown from the progenitor star long before the GRB. The CBs' electrons Compton up-scatter this 'glory' light into a narrow conical beam of γ rays along the CBs' direction of motion. Each CB produces a single GRB pulse. An X-ray 'flare' coincident in time with a prompt γ -ray pulse is simply its low-energy part. The natural explanation of flares ending the prompt emission and during the early time afterglow is the same: ICS of glory photons

by the electrons of CBs ejected in late accretion episodes of fall-back matter on the newly formed central object. Early-time X-ray flares without an accompanying detectable γ -ray emission are usually IC flares (ICFs) produced by CBs with relatively smaller Lorentz factors, due to weakening activity of the engine: As the accretion material is consumed, one may expect the ‘engine’ to have a few progressively-weakening dying pangs. Like the lightcurves of the prompt GRB pulses, the lightcurves of ICFs exhibit a rapid softening during their fast decline phase (see, e.g., the XRT hardness ratio reported for Swift GRBs in the Swift lightcurve repository, Evans et al. (2007, 2009)).

In the CB model, each IC flare (ICF) is followed by the emission of SR flare (SRF) from the encounter of the CB with the wind/ejecta, which was blown from the progenitor star long before the GRB (see Fig. 1). Because of time-aberration in the observer frame, these SRFs appear to have only short lag-times relative to the corresponding ICFs. Below their peak energy, the spectral behaviour of the ICS pulses/flares is roughly $F_\nu \sim \nu^0$, while the SR emission from fast cooling electrons has typically $F_\nu \sim \nu^{-1.1}$. Thus, while the prompt keV-MeV pulses/flares are dominated by ICS of glory light, the ‘prompt’ optical emission is dominated by SR. As the glory extends into the wind, often the SR emission begins before the ICs pulse/flare has ended.

The initial expansion of the CBs and the slow-down of the leading ones by the circum-burst matter may merge most of them into a single leading CB (Dar and De Rújula 2004; Dado et al. 2009a) during the afterglow phase. Its collimated beam of the prompt gamma rays ionizes the matter in front of it. The ions continuously impinging on a CB with a relative Lorentz factor $\gamma(t)$, where $\gamma(t)$ is the bulk motion Lorentz factor of the CB, generate within it an equipartition turbulent magnetic field. The intercepted electrons are isotropized and Fermi accelerated by these fields and emit isotropic synchrotron radiation in the CB’s rest frame, which is Doppler boosted and beamed relativistically into a narrow cone with a typical opening angle $\sim 1/\gamma(t)$ in the observer’s rest frame. Late SRFs are produced mainly when the CBs encounter winds or density bumps along their path first from the progenitor star and later in the interstellar medium (ISM). The lightcurve of these flares depends on the unknown density profile of the encountered wind/density bump that cannot be predicted a-priori. But, both the early-time and the late-time SRFs have a typical SR spectrum and a weak spectral evolution that are quite different from those of the accretion induced ICFs and can be used to identify their origin – late ejection episodes from the central engine or density bumps.

In the CB model, short hard bursts (SHBs) are also produced by bipolar jets of plasmoids ejected in mergers of compact objects in close binary systems such as neutron stars merger (Goodman et al. 1987) or in mass accretion episodes on compact objects in close bi-

nary systems, or in phase transitions in compact stars (neutron stars, hyper stars and strange quark stars) (Dado et al. 2009b). Bipolar ejections in late accretion episodes or phase transitions after cooling and loss of angular momentum probably produce the observed ICFs in SHBs, and SR radiation from encounters with winds/density bumps produces SRFs.

Flares were routinely included in the CB model description of the afterglows of GRBs and SHBs (Dado et al. 2002, 2004, 2009a,b). They were calculated from the master formulae of the model, which describe well the prompt ICS emission and the emission of SR at all times. It was shown that ICS explains successfully both the prompt keV-MeV pulses and the X-ray flares ending the prompt emission, while the SR emitted in the collision of the jet of CBs with the wind/ejecta from the progenitor star explains well the prompt optical flares measured with robotic telescopes in very bright GRBs (Dado et al. 2009a; Dado and Dar 2008). However, attention was focused there on the general properties of the prompt emission and the smooth afterglow, rather than on flares during the afterglow phase. Moreover, in many GRB afterglows, flares are weak, or are blended, or are not well sampled, and their properties could neither be inferred reliably from the AG lightcurve nor used reliably to test theoretical models. The situation concerning prominent X-ray flares observed by the Swift XRT is different. They are well resolved and their spectral properties are much better measured. In this paper we focus our attention on GRB X-ray and optical lightcurves with prominent flares. In particular, we compare the CB model lightcurves and their spectral evolution with a representative set of X-ray and optical lightcurves measured with the Swift XRT, and with ground-based robotic telescopes and Swift UVO in space, respectively, which have prominent flares that are well sampled. Such a comparison provides stringent tests of both the CB model and its interpretation of the origin of prompt emission pulses in GRBs, their afterglows and the early and late time flares in their lightcurves. We show that the CB model correctly predicts their main observed properties, and reproduces well their entire lightcurves and spectral properties. For completeness, we first summarize the relevant master formula of the CB model and their simplified forms that we later use in our analysis of the X-ray and optical lightcurve of GRBs.

2. ICS flares

In this section we summarize the master formula of the CB model for the pulse shape and spectral evolution of ICS pulses/flares (see Dado et al. (2009a) and references therein for their derivation). Let t denote the time in the observer frame after the beginning of a flare. The light-curve of a flare, produced by the electrons in the CBs by ICS of thin bremsstrahlung photons filling the cavity formed by a wind blown by the progenitor star

long before the GRB, is generally well approximated by (Dado et al. 2009a):

$$E \frac{d^2 N_\gamma}{dt dE}(E, t) \approx A \frac{t^2/\Delta t^2}{(1 + t^2/\Delta t^2)^2} e^{-E/E_p(t)} \propto e^{-E/E_p(0)} F(E t^2), \quad (1)$$

where A is a constant that depends on the CB's baryon number, Lorentz and Doppler factors, and on the density of the glory light and on the redshift and distance of the GRB, and $E_p(t)$, the peak energy of $E d^2 N_\gamma/dE dt$ at time t , is given roughly by:

$$E_p(t) \approx E_p(0) \frac{t_p^2}{t^2 + t_p^2}, \quad (2)$$

with t_p being the time (after the beginning of the flare) when the ICS photon count-rate reaches its peak value. For $E \ll E_p$, it satisfies $E_p(t_p) = E_p$ where E_p is the peak energy of the time-integrated spectrum of the flare. Thus, in the CB model, each ICS pulse in the GRB lightcurve is described by four parameters, A , $\Delta t(E)$, $E_p(0)$ and the beginning time of the pulse when t is taken to be 0.

Eq. (1) with E_p given by Eq. (2) describes well the shape and the spectral evolution of GRB pulses and of early-time X-ray flares. In particular, it correctly describes their rapid spectral softening during their fast decline as demonstrated in Figs. 2c,f, 3b and 7d, and in Dado et al. (2008b) for many more cases.

If absorption in the CB is dominated by free-free transitions, then $\Delta t(E) \propto E^{-0.5}$, and for $E \ll E_p$ the lightcurve of an ICF is approximately a function of $E t^2$ (the 'E t^2 ' law'), with a peak at $t = \Delta t$, a full width at half maximum, FWHM $\approx 2 \Delta t$ and a rise time from half peak value to peak value, RT ≈ 0.30 FWHM independent of E. Note that the approximate $E t^2$ law makes the fast decline sensitive only to the product $E_p t_p^2$ and not to their individual values. This degeneracy in the pulse shape can be removed by inferring E_p from the broad band spectrum of the ICF.

The late-time decay of the energy flux of the prompt emission pulses and ICFs in an energy band $[E1, E2]$, which follows from Eq. (1), is given approximately by:

$$\int_{E1}^{E2} E \frac{d^2 N_\gamma}{dt dE}(E, t) dE \approx A \frac{E_p(t) \Delta t^2}{t^2} [e^{-E1/E_p(t)} - e^{-E2/E_p(t)}]. \quad (3)$$

Thus, for the Swift XRT lightcurves where $E1 = 0.3$ keV and $E2 = 10$ keV, as long as $E_p(t) \gg E2 \geq E1$, the energy flux in an ICS pulse/flare decays like t^{-2} until it is taken over by the SR afterglow. When $E_p(t) \gg E1$ but $E_p(t) \lesssim E2$ the energy flux decays like t^{-4} , and when $E_p(t) \lesssim E1$ the energy flux decays like $t^{-4} e^{-E t^2/2 E_p t_p^2}$.

For a single ICF beginning at $t=0$, which is superimposed on a smooth SR afterglow, the effective photon spectral index $\Gamma(E, t) \equiv d \log(dN/dE)/d \log E$ is given approximately by

(Dado et al. 2008b):

$$\Gamma(E, t) \approx [1 - \beta_g + E/E_p(t)]\Theta(t_{AG} - t) \Theta(t) + \Gamma_{SR} \Theta(t - t_{AG}), \quad (4)$$

where t_{AG} is the time when the SR afterglow takes over the ICS emission, $\beta_g \approx 0$ for a glory with thin thermal bremsstrahlung spectrum, and Γ_{SR} is the best fit photon spectral index of the smooth X-ray AG.

All the above properties are clear fingerprints of ICFs produced by highly relativistic CBs fired in mass accretion episodes on the newly formed compact central object. Moreover, the observations of X-ray flares indicate that their widths are proportional to their emission time t_f after the GRB trigger. In the CB model, this implies that their peak energy, equivalent isotropic gamma ray energy and peak luminosity decrease like $E_p \propto t_f^{-1}$, $E_{iso} \propto [(1+z)/t_f]^2$ and $L_p \propto [(1+z)/t_f]^3$.

3. The SR lightcurve

In the CB model, the lightcurve in the observer frame of the SR emitted by a CB is given by the master formula (Dado et al. 2002, 2009a):

$$F_\nu[t] \propto A(\nu, t) \frac{n(t) R(t)^2 \gamma(t)^2 \delta(t)^4}{\nu_b(t)} \left[\frac{\nu}{\nu_b(t)} \right]^{-1/2} \left[1 + \frac{\nu}{\nu_b(t)} \right]^{(1-p)/2}, \quad (5)$$

where t is the time after the ejection of the CB, $R(t)$ is its radius, n is the density along its trajectory, $A(\nu, t)$ is the attenuation of radiation along the line of sight to it, $\nu_b(t)$ is the typical frequency in the observer frame of the SR emitted by the electrons that are swept into it at time t with a relative Lorentz factor $\gamma(t)$,

$$\nu_b(t) \propto \frac{n^{1/2} \gamma(t)^3 \delta(t)}{1+z}, \quad (6)$$

and $p \sim 2.2$ is the spectral index of the Fermi accelerated electrons in it.

3.1. The early time SRFs

The SR radiation that is emitted from the encounter of a CB with the wind/ejecta of the progenitor star, with a density profile $n(r) \propto e^{-a/(r-r_w)}/(r-r_w)^2$ for $r > r_w$ and $n(r) = 0$ for $r < r_w$, follows from Eq. (5) and is given approximately by Dado et al. (2009a):

$$F_\nu \propto \frac{e^{-a/t} t^{1-\beta}}{t^2 + t_{exp}^2} \nu^{-\beta}, \quad (7)$$

where $t = T - T_w$ with T being the time after trigger and T_w the time at the CB-wind encounter, t_{exp} is the typical slow-down time of the fast CB expansion, $\beta = \Gamma - 1$, and the exponent describes the decreasing attenuation of the emitted radiation when the CB penetrates the wind and/or the initial rise in the wind density due to an exponential cutoff of the wind ejection.

Note that for $t^2 \gg t_{exp}^2$ the asymptotic decline of an SRF is a simple power law (Dado et al. 2003),

$$F_\nu[t] \propto t^{-\Gamma} \nu^{-\Gamma+1}, \quad (8)$$

while that of an ICF is,

$$F_\nu[t] \propto t^{-2} E^{-\beta_g} e^{-E/E_p(t)} \sim t^{-2} E^{-\beta_g} e^{-E(t^2+t_p^2)/2 E_p t_p^2}. \quad (9)$$

Thus, ICFs and SRFs may be distinguished by their different tempo-spectral evolution.

In the X-ray band, early-time ICFs are usually much brighter than their following SRFs. But, due to their rapid late-time decay, occasionally the $\sim t^{-\Gamma}$ tail (Eq. 8) of the SRF, which follows an ICF, can be seen before the plateau/shallow decay phase of the early-time X-ray AG takes over (see, e.g., Fig. 3 in Dado et al. (2009a)).

The early time SR has usually $\beta_{OX} \sim 0.75$ and F_ν that decreases strongly between the optical and the X-ray band. Consequently, although ICS dominates the prompt X-ray emission, in the optical band SRFs are usually much brighter than their preceding ICFs, which typically have $\beta \sim 0$ around their peak time. Consequently, optical flares are usually SRFs. The evolution of the effective spectral index during an optical SRF that follows from Eq. (5) has the simple form,

$$\beta \equiv \frac{d \log F_\nu[t]}{d \log \nu} = 1/2 + (\beta_X - 1/2) \frac{\nu}{\nu + \nu_b}. \quad (10)$$

In early-time optical SRFs, ν_b that is initially below the optical band can cross above it as n of the wind/ejecta increases and then cross back as the density decreases. Such a change in β_O , from $\beta_O \sim \beta_X$ towards $\beta_O \sim 1/2$ and back to $\beta_O \sim \beta_X$, has been observed in some early time optical flares, e.g., in GRB 071031 (Kruhler et al. 2009).

3.2. The late-time SR afterglow

When the merged CBs coast through the constant-density ISM, their SR in the X-ray band is well above the cooling frequency of the Fermi accelerated electrons and their unabsorbed AG as given by Eq. (5) reduces to (Dado et al. 2009a):

$$F_{ISM}[\nu, t] \propto \gamma(t)^{3-\beta_X} \delta(t)^{3\beta_X+1} \nu^{-\beta_X} \quad (11)$$

where $\delta = 1/\gamma(1 - \beta \cos\theta)$ is their Doppler factor with θ being the angle between the line of sight to the CBs and their direction of motion. For $\gamma^2 \gg 1$ and $\theta^2 \ll 1$, $\delta \approx 2\gamma/(1 + \gamma^2\theta^2)$ to an excellent approximation. In the CB model the canonical value of the spectral index well above the bend frequency ν_b has the value $\beta_X \approx 1.1$. For a CB of a baryon number N_B , a radius R and an initial Lorentz factor γ_0 , relativistic energy-momentum conservation yields the deceleration law of the CB in an ISM with a constant density n (Dado et al. 2009a):

$$\gamma(t) = \frac{\gamma_0}{[\sqrt{(1 + \theta^2 \gamma_0^2)^2 + t/t_0} - \theta^2 \gamma_0^2]^{1/2}}, \quad (12)$$

with $t_0 = (1+z) N_B/8cn\pi R^2 \gamma_0^3$. As can be seen from Eq. (12), γ and δ change little as long as $t \ll t_b = [1 + \gamma_0^2 \theta^2]^2 t_0$, and Eq. (11) yields the ‘plateau’ phase of ‘canonical AGs’ (Nousek et al. 2006). For $t \gg t_b$, γ and δ decrease like $t^{-1/4}$. The transition $\gamma_0 \rightarrow \gamma_0(t/t_0)^{-1/4}$ around t_b induces a bend, the so called ‘jet break’, in the synchrotron AG from a plateau to an asymptotic power-law decay,

$$F_{ISM}[\nu, t] \propto t^{-\beta_X - 1/2} \nu^{-\beta_X}. \quad (13)$$

Thus, the shape of the entire lightcurve of the SR afterglow from a CB that enters the constant density ISM depends only on three parameters, the product $\gamma_0 \theta$, the deceleration parameter t_0 (or the break time t_b) and the spectral index β_X . The post break decline is given by the simple power-law (Eq. 13) independent of the values of $\gamma_0 \theta$ and t_b . In cases where t_b is earlier than the beginning of the XRT observations or is hidden under the prompt emission, the entire observed lightcurve of the AG has this asymptotic power-law behaviour (Dado et al. 2008a).

3.3. Late-time SRFs

The lightcurve of late-time SRFs strongly depend on the density profile of the density bumps. For a wind-like density jump $n \propto e^{-a_w/(r-r_w)}/(r-r_w)^2$ beyond $r=r_w$, the lightcurve is given by Eq. (7). Such a density profile is expected for the boundaries of star formation regions where GRBs usually take place. At late times both the optical and the X-ray bands are above the bend frequency, $\beta_O \approx \beta_X$, and the asymptotic decline of the corresponding late-time SRF is given by:

$$F_\nu[t] \propto t^{-\Gamma} \nu^{-\Gamma-1}, \quad (14)$$

where $t = T - T_w$ is the observer-time after the CB has reached r_w . At late times, the bend frequency is well below the optical band and remains so during the crossing of density bumps. Thus, no detectable spectral variation is expected in late-time SRFs.

3.4. Correlations

Because of the large bulk motion Lorentz factors of the jets of CBs, Doppler boosting, relativistic beaming and time aberration yield strong dependence of their observed radiations on γ and δ . This dependence dominates the flare observables and can be used to correlate triplets of independent flare observables without knowing the exact values of γ and δ . Moreover, many independent observables depend on the same combinations of γ and δ , which results in pair correlations. Finally, due to selection effects, various observables depend strongly only on the Lorentz factor or on the Doppler factor, which also yields pair-correlations. These correlations between various radiations, between flare observables and between flare and GRB observables are discussed in detail in Dado and Dar (2010).

4. Case Studies

Although in the CB model early-time optical SRFs follow the X-ray ICFs, they have a different origin and a different tempo-spectral evolution. Thus, we shall compare separately the observational data on X-ray flares and optical flares and the CB model predictions.

4.1. X-ray flares

In the CB model, the X-ray emission in GRBs, XRFs and SHBs during the prompt emission phase is a sum of X-ray flares that are part of their prompt gamma ray pulses. That has been shown repeatedly in CB model publications (see, e.g., Dado et al. (2009a,b)) and independently by many other authors. We have also shown that the fast decline phase of their prompt emission with its rapid spectral softening is just the tail of the last prompt emission pulses, because the exponential factor in Eq. (1) suppresses very fast the relative contribution of the earlier pulses by the time the data sample the later pulses or flares. This is demonstrated in Figs. 2a,b,c where we compare between the ‘canonical X-ray lightcurve’ (Nousek et al. 2006) of GRB 060729 and the evolution of its spectral index as inferred by Zhang et al. (2007) and the CB model descriptions of these lightcurves. This has already been demonstrated in detail in Dado et al. (2008b, 2009a) for many other GRBs and XRFs. It is also the case for SHBs as shown in Figs. 2e,2f for SHB 050724 and in Dado et al. (2009b) for many other SHBs. GRBs with a non-canonical X-ray AG, are simply GRBs where the emission of SR begins to dominate the X-ray lightcurve before the fast decline phase of the prompt emission. Such a case is shown in Fig. 3d where we compare the XRT lightcurve of GRB 060418 and its CB model description. Many other cases are shown in Dado et al.

(2008b, 2009a,b).

In order to have a stringent test of the CB model interpretation of X-ray flares during the afterglow phase of GRBs, we have selected a sample of 14 GRBs with X-ray lightcurves that are reported in the Swift/XRT GRB lightcurve repository (Evans et al. 2007, 2009) and have well sampled prominent flares during their AG phase. This sample includes GRBs 050502B, 050916, 060526, 060929, 070704, 080506, 080607, 080810, 080906, 081102, 090417B, 090621A, 090709A, and the SHB 050724. For all these GRBs we have fitted the entire XRT lightcurve with the master formulae of the CB model. In order to minimize the number of adjustable parameters in the theoretical lightcurves, we adopted the standard simplifying CB model assumptions (Dado et al. 2009a): The burst environment is a cavity full of thin bremsstrahlung optical photons (glory light) enclosed within a wind/ejecta that have a density profile $n \propto e^{-a_w/(r-r_w)}/(r-r_w)^2$ beyond r_w until the density is taken over by the constant density of the ISM. The CBs were taken to be well separated during the prompt emission phase and to be well represented by a single effective CB during the afterglow phase. The latest one or two observed pulses/flares in the prompt emission were assumed to dominate its fast decay. This fast ICF decay is overtaken by the tail of the SR emission from the encounter of the CBs with the wind/ejecta as given by Eq. (7), or by the plateau phase of the SR afterglow emitted from the decelerating CB in the constant-density ISM. The smooth afterglow was calculated from Eqs. (11), (12), using best fit values of the normalization, $\gamma_0 \theta$, t_0 , and $p/2=\beta_X$ with β_X within the error range reported for $\Gamma = \beta_X + 1$ in the Swift X-ray repository (Evans et al. 2009).

Prominent X-ray flares during the afterglow with a rapid spectral softening during their decline phase were assumed to be ICS pulses/flares. Such flares were superimposed on the CB model smooth SR afterglow. Flares with a constant hardness ratio similar to that of the smooth SR afterglow were assumed to be SRFs. They were generated by introducing density bumps with a windy profile into the master formula of the SR lightcurve (Dado et al. 2009a).

The fitted parameters of the CB model descriptions of the 14 X-ray light curves of the above GRBs are listed in Tables 1,2. When only the tail of the SRF was visible we used its parameter-free asymptotic form, Eq. (8). Because of the use of simplifying assumptions, the values of the parameters may be effective values and not true values. Therefore, we refer to the CB model fits as ‘descriptions’ rather than as best fit predictions. In order to avoid repetitions and an excessively long section, we limit our detailed discussion to three representative cases, GRB 050502B representing long soft GRBs, SHB 050724 representing short hard bursts, and the recent peculiar GRB 090709A with a suspected 8 s periodicity in its prompt emission.

GRB 050502B was studied in detail by Falcone et al. (2006). The XRT began taking data 63 s after the BAT trigger and followed its X-ray lightcurve until 10.6 days after burst. The measured lightcurve in the 0.3-10 keV band is shown in Figure 2a. Following an initial low-flux level, the XRT detected a giant X-ray flare, which began at 345 ± 30 s, reached a peak value around 770 s, with intensity more than 500 times larger than that of the underlying afterglow. The fluence of the flare, $(1.0 \pm 0.05) \times 10^6$ erg cm⁻² in the 0.2-10.0 keV energy band, exceeded that of the prompt emission measured with the Swift BAT in the 15-350 keV energy band. After several hours, two weaker flares in the X-ray emission occurred consecutively beyond which the decay of the X-ray lightcurve became steeper. Except for the giant flare, the spectrum of the afterglow and the two late flares was well fit by a power-law with a photon spectral index $\Gamma=1.945$ (+0.077, -0.100) (Evans et al. 2007, 2009). The spectrum of the flare was well fit with a power-law with an exponential cutoff; however, due to its non detection by the BAT, its value could not be well determined from the spectrum measured only by the XRT. The photon spectral index of the giant flare before peak-time was $\Gamma \approx 1$, much harder than that measured before and after the flare. During the fast decline phase of the flare, a rapid spectral softening took place and the spectral index increased rapidly to a value well above the constant value of the smooth afterglow.

CB model fits to the X-ray lightcurve of GRB 050502B and the evolution of its spectral index are shown in Figs. 3a,b. They show that the observed lightcurve and spectral evolution of the giant X-ray flare are well described by the master formula (Eq. (1)) of the CB model for an ICF. As can be seen in Figs. 3a,b, the fast decay and spectral softening stopped simultaneously when the AG was taken over by the smooth SR from the decelerating CB in an ISM of a constant density. The late-time afterglow shows two flares superimposed on the smooth AG, similar to those observed in many long GRBs. Their spectrum, which is similar to the smooth AG, suggests that they were produced by enhancement of the emitted SR when the CB encountered density bumps in its voyage through the host's ISM. Such late flares with a typical SR spectrum and little spectral evolution produced by density bumps along the CB trajectory in the ISM add no specific information on the origin of GRBs.

SHB 050724 at redshift $z = 0.257$ was studied in detail by Campana et al. (2006), citet-Grupe2006 and Malesani et al. (2007). The Swift BAT triggered on the burst at 12:34:09 UT on July 24, 2005. The burst had $T_{90}=3.0 \pm 1.0$ s, but most of the energy of the initial SHB was released in a hard spike with a duration of 0.25 s. The bulk of the burst energy was not emitted in the short initial spike but in an extended soft emission component that lasted ~ 150 s. Swift XRT began observing the afterglow 74 s after the BAT trigger. The Chandra X-ray observatory performed two observations, two days and about three weeks after the burst. The complete X-ray lightcurve is shown in Fig. 2e. It has a rapid decay with a fast spectral softening ending with a sharp transition to a shallower decay with a much

harder power-law spectrum, $\Gamma = 1.79 \pm 0.12$ (Swift repository, Evans et al. (2009)). The AG steepens gradually into a late power-law decay. A large flare superimposed on the canonical lightcurve occurred around 50 ks after burst with a fluence of $\sim 7\%$ of that of the prompt burst. The flare has been detected also in the optical and NIR bands, e.g., Malesani et al. (2007). Spectral analysis of the XRT data (Campana et al. 2006) showed no evolution during the afterglow phase, including the large late flare. Spectral analysis of the Chandra observations from the fading tail of this flare confirmed this result (Grupe et al. 2006). The burst took place 2.5 kpc (in projection) from the center of an elliptical host galaxy (Malesani et al. 2007).

CB model fits to the X-ray lightcurve of SHB 050724 and the evolution of its spectral index are shown in Figs. 2e,f. The initial fast decay with a rapid spectral softening is described in the CB model by the tail of an ICF. As can be seen in Figs. 2b,2c, the fast decay and spectral softening stopped simultaneously when the AG was taken over by the SR from the decelerating CB in an ISM of a constant density. As expected, the late-time SR afterglow is similar in shape to the SR afterglow of long GRBs. Also the late-time flare superimposed on the canonical lightcurve is similar to those observed in many long GRBs. Its spectrum, which is similar to the smooth AG, suggests that it was produced by enhancement of the emitted SR when the CB encountered a density bump in its voyage through the host's ISM. The Chandra data show that the canonical AG continued to decay after the flare with the same slope and the same spectral index, $\beta_X = 0.79 \pm 0.15$, as that of the AG before the SRFs. As shown in Fig. 2e, the complete XRT lightcurve is well described by the CB model. Moreover, the CB model relation for the asymptotic decline of the smooth AG is well satisfied: The temporal behaviour of the smooth AG was best fit with $p=1.56$, implying an unabsorbed spectral index, $\beta_X = p/2 = 0.78$, in agreement with that inferred from the XRT and Chandra observations. The observed elliptical host galaxy of SHB 050724 was argued to provide strong support for a neutron star merger origin of this SHB. But, it was pointed out that neutron star mergers do not produce the late accretion episodes needed to power a late central activity that could produce the large flare around 50 ks after burst (Grupe et al. 2006). In the CB model, a late flare with a typical SR spectrum and little spectral evolution is produced by density bumps along the CB trajectory in the ISM. Such flares neither rule out nor support any specific origin of the SHB.

GRB 090709A triggered the Swift BAT on July 9, 2009 at 07:38:34 UT (Morris et al. 2009). Its prompt emission lightcurve within 100 seconds after trigger appeared to show a quasi periodic variation with a period of ~ 8 seconds (Markwardt et al. 2009), which may have also seen in independent measurements of its lightcurve with Konus-Wind (Golenetskii et al. 2009), INTEGRAL (Gotz et al. 2009), and Suzaku (Ohno et al. 2009). The Swift XRT began

its follow-up observations 68 seconds after the BAT trigger (Morris et al. 2009). However, analysis by Mirabal and Gotthelf (2009) of the XRT data during 79-469 seconds after the BAT trigger did not reveal any significant periodicity. From deep optical observations that did not detect its host galaxy, it was concluded that GRB 090709A took place either in the Milky Way or at a redshift between 8 and 10 (Castro-Tirado et al. 2009). The large redshift and the fluence of $9.1 \times 10^{-5} \text{ erg cm}^{-2}$ measured with Konus-Wind in the 20 keV-3 MeV energy range imply an isotropic equivalent gamma-ray energy between 8.6×10^{54} and $1.1 \times 10^{55} \text{ erg cm}^{-2}$, which makes GRB 090709A more luminous than any GRB with known redshift.

Figs. 6e,f present a comparison between the XRT lightcurve of GRB 090709A and its CB model description assuming it was an ordinary GRB. The early time flare around $t=90$ seconds probably is the X-ray part of the prompt emission pulse with a peak around 87 seconds in the Swift BAT lightcurve that is slightly delayed relative to the gamma-ray peak, as expected from the Et^2 law of the CB model. Its fast decline and rapid softening are those expected from an ICF. They are taken over by SR around 150 seconds after the BAT trigger. The next 3 peaks probably are SR peaks as suggested by their shape and their hardness ratio that is roughly the same as that of the SR afterglow. The best fit CB model lightcurve of the smooth AG yields $p=2.16$, which, in the CB model, implies $\beta_X = 1.082$, in good agreement with the best fit spectral index reported in the Swift repository (Evans et al. 2009), $\beta_X = \Gamma - 1 = 1.081 (+0.076, -0.074)$. All together, GRB 090709A looks like a normal GRB with a normal early time flaring activity that took place at a relatively very large redshift, and its X-ray lightcurve is well reproduced by the CB model.

4.2. Optical flares

The CB model predictions for early-time and late-time flares in the optical lightcurves of GRBs are compared with observations for a representative set of GRBs in Figs. 7-11. For all these GRBs we show both their measured optical and X-ray lightcurves (if available) and their CB model descriptions with the parameters listed in Tables 1-5.

Only in a very few bright GRBs was the prompt optical emission resolved into separate flares. Two such cases, GRB 080319B (Wozniak et al. 2009) and GRB 071003 (Perley et al. 2008) are shown in Fig. 7. In most GRBs and XRFs, the prompt optical emission that appears as a single extended flare, probably, is a sum of unresolved flares. Cases where the prompt optical flare was partially resolved into a sum of flares or where there is clear evidence for overlapping flares are, e.g., GRB 080330 (Guidorzi et al. 2009), XRF 071031 (Kruhler et al. 2009), GRB 061007 (Rykoff et al. 2009), which are shown in Figs. 8,9. In

most GRBs where the prompt optical emission was detected with robotic telescopes from the ground or from space (with the Swift/*UVO*), the prompt emission appears like a single flare, probably as a result of either strongly overlapping flares, or insufficient temporal resolution due to low statistics, or because the prompt emission did consist of a single flare. Examples of GRBs with a ‘single’ prompt optical flare are 990123 (Akerlof et al. 1999), 030418 (Rykoff et al. 2004), 050820A (Vestrand et al. 2006), 081203A (Kuin et al. 2009), 090102 (Gendre et al. 2009), 090618 (Li et al. 2009) and 091029 (LaCluyze et al. 2009), which are shown in Figs. 9-11. Examples of bright GRBs with well resolved late-time optical flares include GRB 030329 (Lipkin et al. 2004) and GRB 060206 (Wozniak et al. 2006) shown in Fig. 11f. However, in order not to inflate this paper, only GRB 080319B, XRF 071031, GRB 061007 and GRB 990123 are discussed here in detail.

GRB 080319B at redshift $z = 0.937$, the brightest GRB observed so far, was simultaneously detected by the Swift-Burst Alert Telescope (BAT) and the Konus gamma-ray detector aboard the Wind satellite (Racusin et al. 2008; Golenetskii et al. 2008). The location of GRB 080319B was fortuitously only 10° away from GRB 080319A, which was detected by Swift less than 30 minutes earlier, and allowed several wide field telescopes to detect the optical emission of GRB 080319B instantly. It started after the beginning of the prompt keV-MeV emission and it peaked 26 s after the Swift trigger at magnitude $V = 5.3$ (Racusin et al. 2008; Wozniak et al. 2009) visible to the naked eye. The extreme brightness of the burst and its gamma-ray, X-ray and *UVOIR* afterglows led to a flurry of follow-up observations with a variety of space- and ground-based telescopes, which were summarized by Bloom et al. (2008); Racusin et al. (2008); Wozniak et al. (2009). Its isotropic equivalent gamma-ray energy release was $E_{iso} \approx 1.3 \times 10^{54}$ erg, similar to that of GRB 990123. The fast spectral variation of its hard X-ray and gamma ray emission was well parametrized with an exponentially cut-off power-law with a cut-off energy that was strongly correlated with the peak structure of the lightcurve and a low-energy photon spectral index, $\Gamma \approx 1$, which changed abruptly into $\Gamma \approx 2.1$ after the fast decay phase of the prompt emission. The optical and gamma-ray lightcurves during the explosion were not correlated (see, e.g., Fig. 1 in Racusin et al. (2008)): The onset of the optical emission lagged behind the gamma ray emission by several seconds and decayed more slowly at the end of the prompt emission. The typical time scales of their temporal variability were entirely different. The extremely bright optical emission could not be reconciled with a single emission mechanism - extrapolating the gamma-ray spectrum to the optical band underestimates the optical flux by more than 4 orders of magnitude. Their spectra were also quite different. Contrary to fireball (FB) model expectations, the X-ray and *UVO* afterglow lightcurves were also chromatic, with no obvious ‘jet breaks’ and with spectral and temporal power-law decays that did not satisfy the closure relations expected in the FB model (see, however, Bloom et al. (2008); Racusin et al. (2008); Wozniak et al. (2009);

Kumar et al. (2008) for attempts to reconcile the observations with the fireball model).

The prompt γ -ray and hard X-ray emission in GRB 080319B is composed of many narrow peaks (see Fig. 1 in Racusin et al. (2008)), most of which are not well resolved. Its 0.3-10 keV X-ray lightcurve measured with the Swift XRT (Racusin et al. 2008) and its CB model description assuming a constant ISM density until around $t \sim 4 \times 10^5$ s, presumably when the CB escaped the star formation region into the halo of the host galaxy, are shown in Fig. 7a. The best fit parameters are listed in Table 1. The late time temporal decay of the X-ray AG is well described by a power-law with $\alpha_X = 1.54 \pm 0.04$, except around 40 ks, where the lightcurve is poorly sampled. This value of α_X satisfies well the CB model closure relation $\alpha_X = \beta_X + 1/2 = 1.53! \pm 0.064$. As expected for GRBs with large measured E_p , E_{iso} and L_p (Dado et al. 2008b), no AG break was observed in the XRT lightcurve before 6×10^5 s. The wiggling of the measured lightcurve around a power-law decay is probably due to variations in the ISM density along the CB trajectory, which we have not tried to parametrize. A late-time SRF with a typical late-time decay $\sim (t - t_f)^{-2.1}$ probably was observed around 6×10^5 s.

In Fig. 7b we compare the measured R -band (and V band renormalized to the R band) lightcurve of GRB 080319B (Racusin et al. 2008) and its CB model description assuming that the initially expanding 3 CBs merged into a single CB by the end of the prompt ICS emission of gamma-rays and hard X-rays around 300 s (observer time), which decelerates in roughly a constant density ISM. The afterglow parameters are listed in Table 3. The ‘missing jet break’ probably is hidden under the prompt emission. Shown also is the contribution to the R -band afterglow from an SN akin to SN1998bw (Galama et al. 1998b) displaced to the GRB site.

The early-time optical emission that was resolved into three prominent peaks and its CB model description in terms of 3 SR peaks, each one described by Eq. (7) with the parameters listed in Table 3, are compared in Fig. 7c. The decay of the prompt emission can also be reproduced assuming a single CB crossing 3 wind shells, which were ejected by the progenitor star long before its SN explosion, rather than 3 CBs crossing a continuous pre-supernova wind blown by the SN progenitor.

In Fig. 7d, the observed evolution of the spectral index in the 15-150 keV band during the prompt emission and the afterglow (Racusin et al. 2008) are compared with that predicted by the CB model. The predicted sharp transition from the prompt emission, which is dominated by ICS of thin bremsstrahlung ($\Gamma \approx 1$), to SR ($\Gamma_x \approx 2.1$), which dominates the emission once the CBs encounter the progenitor’s wind/ejecta, is clearly observed.

XRF 071031 was studied in detail by Kruhler et al. (2009). The Swift/XRT began follow-

up observations of XRF 071031 103 s after the burst. The early XRT lightcurve (XRT lightcurve repository, Evans et al. (2009)) is dominated by bright flares at around 120 s, 150 s, 200 s, 250 s and 450 s. The late X-ray data exhibit re-brightenings at 5.5 ks, 20 ks and 55 ks superimposed on a smooth AG. The complete XRT lightcurve was reproduced with the CB model, assuming 7 early-time ICFs plus two late time SRFs superimposed on a smooth SR afterglow. Their parameters are listed in Table 2. As shown in Figs. 8c,d the CB model describes well the very complex XRT lightcurve ($\chi^2/dof = 431/426$). The values of the photon spectral index of the late time afterglow, $\Gamma_X=1.86 (+0.14, -0.15)$, and the index of the late time power-law decay, $\alpha_X = 1.4 \pm 0.1$, which were inferred from the Swift/XRT observations (Swift XRT lightcurve repository, Evans et al. (2009)), satisfy well the CB model closure relation, $\alpha_X = \Gamma_X - 1/2$.

The emission in the optical band was detected and followed up from the ground in automated observations by GROND (Kruhler et al. 2009) with good temporal resolution, which began 225 s after burst and lasted nearly 7 h. The white lightcurve obtained by adding the various optical bands, in order to increase sensitivity, shows a broad peak with clear deviations from a power-law rise and decay. Fig. 8e shows the CB model description of this lightcurve in terms of strongly overlapping 4 SRFs following their preceding ICFs in the X-ray lightcurve. The parameters used in the CB model description are listed in Table 3. Comparison between the optical spectral index lightcurve that was inferred by Kruhler et al. (2009) and the CB model prediction as given by Eq. (10) is shown in Fig. 8f.

GRB 061007 at a redshift $z=1.26$ (Jakobsson et al. 2006), which was detected by Swift, had a T90 duration of 75.3 s in the Swift BAT 15-350 keV band, and consisted of three large peaks with a long faint tail (Markwardt et al. 2006; Sakamoto et al. 2008). The Swift XRT began observations 80 s after the start of the burst. The optical observations began 27 s after the start of the burst by the ROTSE-IIIa robotic telescope (Rykoff et al. 2009). The optical lightcurve shows a sharp rise, brightening by over a factor of 50 in less than 5 s, followed by two peaks and a steady power-law decline. The γ -ray and X-ray lightcurves have multiple peaks that are not contemporaneous with the optical peaks (Rykoff et al. 2009), followed by a steady decline in the X-rays that tracks the optical decline. The three overlapping optical peaks could be the three SRFs following the three large BAT peaks. In Fig. 9c we compare the 0.3-10 keV Swift XRT lightcurve of GRB 061007 (Swift XRT lightcurve repository, Evans et al. (2009)), and its CB model description as the tail of the prompt emission SRFs overtaken around $t=300$ s by a standard AG with an early-time break hidden under the prompt emission. The best fit parameters are listed in Table 1. Note that both the early-time and late-time decays satisfy well the CB model closure relations: $\alpha = \Gamma = 1.884(+0.023, -0.023)$ for the early-time decay and $\alpha = \Gamma - 1/2 = 1.518(+0.087, -0.083)$ for the late-time decay, respectively. In Fig. 9d we compare the optical lightcurve of GRB

061007 as measured by ROTSE-IIIa (Rykoff et al. 2009) and its CB model description in terms of three overlapping SRFs and a standard AG taking over around $t=400$ s. Note that the late-time optical AG also satisfies well the CB model prediction, $\alpha_O = \beta_O + 1/2 = \beta_X + 1/2 = 1.518(+0.087, -0.083)$.

GRB 990123 at redshift $z = 1.600$ (Kulkarni et al. 1999; Andersen et al. 1999) was for a long time the brightest known GRB. It was also the first GRB in which an optical emission was detected during the prompt γ /X-ray emission. GRB 990123 was detected and localized by the Burst And Transient Source Experiment (BATSE) on board the Compton Gamma Ray Observatory (CGRO) in the keV-MeV range and at higher energies by the COMPTEL, OSSE and EGRET instruments (Briggs et al. 1999). It was also detected and localized by the Gamma Ray Burst Monitor (GBM) aboard the BeppoSAX satellite (Maiorano et al. 2005). The lightcurves of the prompt emission in the keV-MeV range showed a complex structure of at least 9 pulses/flares (see Fig. 9a). The prompt optical emission that was detected by the Robotic Optical Transient Search Experiment (ROTSE) at Los Alamos 22 s after the onset of the burst, brightened and peaked at magnitude $V \sim 9$, about 50 s after the GRB onset, and decayed rapidly with time (Akerlof et al. 1999). The prompt optical flare was not resolved into separate flares. It was followed in the *UVONIR* bands with large ground based telescopes (Castro-Tirado et al. 1999; Galama et al. 1999; Kulkarni et al. 1999; Fruchter et al. 1999; Holland et al. 2000) and with the Hubble Space Telescope until it faded to a magnitude $V = 27.7 \pm 0.15$, two months after burst (Fruchter et al. 2000). The broad band γ -ray, X-ray, *UVO* and *NIR* lightcurves of GRB 990123 were reanalyzed recently within the synchrotron fireball (FB) model by Corsi et al. (2005). Essentially they found that the spectral and temporal properties of the prompt optical emission are uncorrelated to the γ and X-ray emission, implying different physical origins, that the optical and X-ray afterglow lightcurves are chromatic contrary to expectations, and that their spectral and temporal power-law decays do not satisfy the closure relations of the FB model.

In Fig. 9a we compare the BATSE multi-peak lightcurve of GRB 990123 in the 20-50 keV channel (Briggs et al. 1999) and its CB model description. The count-rate in the 20-50 keV energy band was calculated from the integral $\int F_\nu dE/E$ using Eq. (1) with the best fit parameters, which are listed in Table 4 for the 9 peaks suggested by the multichannel BATSE data and by the BeppoSAX data (Maiorano et al. 2005). As shown in Fig. 9a, the shape of the peaks and the entire lightcurve are well reproduced by Eq. (1). The 2-10 keV lightcurve of the X-ray afterglow of GRB 990123 that was measured with BeppoSAX (Maiorano et al. 2005) for $t < 2.5$ days (not shown here) was best fit by the CB model with $p = 1.79$, implying $\beta_X = 0.90$, consistent with $\beta_X = 0.94 \pm 0.12$ that was inferred by Maiorano et al. (2005) from their data. The observed temporal power-law decay index of the late-time X-ray afterglow, $\alpha_X = 1.46 \pm 0.04$ (Maiorano et al. 2005), also obeys the CB

model relation , $\alpha_X = \beta_X + 1/2 = 1.44 \pm 0.13$.

In Fig. 9b we compare the observations of the optical lightcurve of GRB 990123 from onset (Akerlof et al. 1999) until late time (Castro-Tirado et al. 1999; Galama et al. 1999; Kulkarni et al. 1999; Fruchter et al. 1999; Holland et al. 2000), normalized to the V -band, and its CB model description as given by Eq. (11) with the afterglow parameters $\gamma\theta = 0.24$, $t_0 = 2250$ s and $p = 1.79$. Due to a gap in the data between 500 s and 15,000 s, the expected transition from a circumstellar density profile $\propto 1/r^2$ to a constant ISM density was not well determined. However, the gradual bending (‘jet break’) of the optical AG to an asymptotic power-law decay, $F_\nu \propto t^{-\beta_O - 1/2} \nu^{-\beta_O}$, is well reproduced with the expected late-time spectral index $\beta_O \sim \beta_X \sim 1.1$.

5. Summary and Conclusions

In the CB model, GRBs, XRFs and SHBs and their afterglows are produced by the interaction of bipolar jets of highly relativistic plasmoids (cannonballs) of ordinary matter, which are ejected in mass accretion episodes on a newly formed compact stellar object, with the radiation and matter that they encounter along their path. As observed in microquasars, each time part of the accretion disk falls abruptly onto the compact object, two jets of cannonballs (CBs) made of *ordinary-matter plasma* with large bulk-motion Lorentz factors are emitted in opposite directions along the rotation axis, wherefrom matter has already fallen back onto the compact object due to lack of rotational support. The prompt γ -ray and X-ray emission is dominated by inverse Compton scattering (ICS) of photons of the glory - a quasi isotropic optical light emitted by the supernova and scattered by the wind/ejecta blown from the progenitor star long before the GRB. The CBs’ electrons Compton up-scatter the glory photons into a narrow conical beam of γ rays along the CBs’ direction of motion. An X-ray ‘flare’ coincident in time with a prompt γ -ray pulse is simply its low-energy part. The early-time X-ray flares without a detectable accompanying γ -ray emission are usually ICFs produced by CBs with relatively smaller Lorentz factors due to a weakening activity of the central engine: As the accretion material is consumed, the ‘engine’ has a few progressively-weakening dying pangs. The lightcurves of ICFs, like those of the prompt emission pulses, exhibit a rapid softening during their fast decline phase. Roughly, the lightcurves are a function of the product $E t^2$ and not of the individual values of the photon energy E and the time t after the beginning of the flare. The peak energy, isotropic equivalent energy and peak luminosity of the ICFs are correlated like those of the prompt GRB pulses.

In the CB model, each ICF is followed by SRF from the encounter of the CB with the wind/ejecta that was blown from the progenitor star long before the GRB. Because of

time-aberration, in the observer frame, these SRFs lag after their preceding ICFs by a short time of the order of the ICS pulse duration. Optical flares are usually much wider than their corresponding gamma/X-ray pulses and overlap, which makes it difficult to associate the early time optical flares with their preceding gamma/X-ray pulses/flares and measure their lag-time. Only in single-pulse GRBs that are bright enough to be detected with robotic telescopes and/or Swift UVO and in very bright GRBs, such as 080319B and 071031, where the optical flares were partially resolved with robotic telescopes, could the predicted association between early time optical flares following gamma/X-ray pulses/flares be tested.

Often the fast decay of an X-ray ICF is taken over by SR of X-rays from the CB encounter with the wind enclosing the glory light before it disappears under the plateau/shallow decay phase of the AG (see, e.g., Figs. 3a,b,c in Dado et al. (2009a)).

Late-time flares are usually SRFs produced by CB encounters with the bumpy boundary of the star formation region, or with density bumps within this region where the GRB took place. Their exact profile is not known a priori but a wind-like profile seems to be a good working hypothesis,

Unlike the empirical parametrizations (such as Band function (Band et al. 1993), cut-off power-law, Beuermann function (Beuermann et al. 1999), broken power-law, segmented power-law, etc.) used in most of the published standard analyses of GRB lightcurves, which have never been properly derived from underlying physical assumptions, the master formulae of the CB model were derived in fair approximations from its underlying physical assumptions. As shown in this paper, the lightcurves and spectral evolution of X-ray flares and optical flares in GRBs, XRFs and SHBs are well described by the master formulae of the cannonball model of GRBs. So far, no new assumptions or modifications of these formulae were needed when applied to well sampled flares in the GRB lightcurves. Probably, in the future, when much more refined data and better sampled lightcurves of GRBs and their AGs will become available, the CB model with its current simplifying assumptions, which were introduced in order to avoid ‘over parametrization’ and make it predictive and falsifiable, will have to be refined in order to reproduce such data with sufficient accuracy.

Acknowledgment. We thank an anonymous referee for useful suggestions and T. Kruhler for making available to us tabulated data of the optical lightcurves of GRB 071031 measured with GROND.

REFERENCES

- Akerlof, C., et al. 1999, *Nature*, 398, 400
- Andersen, M. I., et al. 1999, *Science*, 283, 2075
- Band, D., et al. 1993, *ApJ*, 413, 281
- Berger, E., et al. 2000, *ApJ*, 545, 56
- Beuermann, K., et al. 1999, *A&A*, 352, L26
- Bloom, J. S., et al. 2008, arXiv:0803.3215
- Briggs, M. S., et al. 1999, *ApJ*, 524, 82
- Burrows, D. N., et al. 2005, *Science*, 308, 2005
- Burrows, D.N., et al. 2007, *MNRAS*, 376, 1213, 2007
- Butler, N. & Kocevski, D. 2007, *ApJ*, 663, 407
- Campana, S., et al. 2006, *A&A*, 454, 113
- Castro-Tirado, A. J., et al. 1999, *Science*, 283, 2069
- Castro-Tirado, A. J., et al. 2009, *GCN Circ.* 9655
- Chincarini, G., et al. 2007a, *AdSpR*, 40, 1199
- Chincarini, G., et al. 2007b, *ApJ*, 671, 1903
- Chincarini, G., et al. 2008a, arXiv:0809.1026
- Chincarini, G., et al. 2008b, arXiv:0809.2151
- Corsi, A., et al. 2005, *A&A*, 438, 829
- Dado, S. & Dar, A. 2008, arXiv:0812.3340
- Dado, S. & Dar, A. 2010, arXiv:1001.1865
- Dado, S., Dar, A. & De Rújula, A. 2002, *A&A*, 388, 1079
- Dado, S., Dar, A. & De Rújula, A. 2003, *ApJ*, 593, 961
- Dado, S., Dar, A. & De Rújula, A. 2004a, *A&A*, 422, 381

- Dado, S., Dar, A. & De Rújula, A. 2004b, arXiv:astro-ph/0406325
- Dado, S., Dar, A. & De Rújula, A. 2008a, ApJ, 680, 517
- Dado, S., Dar, A. & De Rújula, A. 2008b, ApJ, 681, 1408
- Dado, S., Dar, A. & De Rújula, A. 2009a, ApJ, 696, 994
- Dado, S., Dar, A. & De Rújula, A. 2009b, ApJ, 693, 311
- Dai, Z. G., et al. 2006, Science, 311, 1127
- Dar, A., et al. 1992, ApJ, 388, 164
- Dar, A. 1998, ApJ, 500, L93
- Dar, A. & De Rújula, A. 2004, Phys. Rep. 405, 203
- Dar, A. & Plaga, R. 1999, A&A, 349, 259
- De Rújula, A. 1987, Phys. Lett. 193, 514
- Evans, P., et al. 2007, A&A, 469, 379.
- Evans, P., et al. 2009, MNRAS, 397, 1177
- Fan, Y. Z., Zhang, B. & Proga, D. 2006, ApJ, 635, L129
- Falcone, A., et al. 2006, ApJ, 641, 1010
- Falcone, A., et al. 2007, ApJ, 671, 1921
- Fruchter, A. S., et al. 1999, ApJ, 519, L13
- Fruchter, A. S., et al. 2000, GCN Circ. 712
- Galama, T. J., et al. 1998a, ApJ, 497, L13
- Galama, T. J., et al. 1998b, Nature, 395, 670
- Galama, T. J., et al. 1999 Nature, 398, 394
- Garnavich, P. M., Loeb, A. & Stanek, K. Z. 2000, ApJ. 544, L11
- Golenetskii, S., et al. 2008, GCN Circ. 7482
- Gendre, B., et al. 2009, arXiv0909.1167

- Golenetskii, S., et al. 2009, GCN Circ. 9647
- Goodman, J., Dar, A. & Nussinov, S. 1987, ApJ, 314, L7
- Gotz, D., et al. 2009, GCN Circ. 9649
- Granot, J., Nakar, E. & Piran, T. 2003, Nature, 426, 138
- Grupe, D., et al. 2006, ApJ, 653, 462
- Guidorzi, C., et al. 2009, A&A, 499, 439
- Holland, S., et al. 2000, A&A, 364, 467
- Jakobsson, P. et al. 2006, GCN Circ. 5716
- King, A., et al. 2005, ApJ 630, 1113
- Kocevski, D., & Butler, N. 2007, ApJ, 667, 1024
- Kruhler, T., et al. 2009, ApJ, 697, 758
- Kuin, N. P. M., et al. 2009, MNRAS, 395, L21
- Kulkarni, S. R., et al. 1999, Nature, 398, 389
- Kumar, P. & Panaitescu, A. 2008, MNRAS, 391, L19
- LaCluyze, A., et al. 2009, GCN Circ. 10107
- Li, W., Perley, D. A. & Filippenko, A. V. 2009, GCN Circ. 9517
- Lipkin, Y. M., et al., 2004, ApJ, 606, 381
- Maiorano, E., et al. 2005, A&A 438, 821
- Mangano, V., et al. 2007, A&A, 470, 105
- Malesani, D., et al. 2007, A&A, 473, 77
- Margutti, R., et al. 2009, arXiv:0910.3166
- Markwardt, C. B. et al. 2006, GCN Circ. 5713
- Markwardt, C. B., et al. 2009, GCN Circ. 9645
- Mirabel, I. F. & Rodriguez, L. F. 1999, ARA&A, 37, 409

- Mirabal, N. & Gotthelf, E. V. 2009, GCN Circ. 9696
- Morris, D. C., et al. 2009, GCN Circ. 9625
- Nousek, J., et al. 2006, ApJ, 642, 389
- Ohno, M., et al. 2009, GCN Circ. 9653
- Pian, E., et al. 1998, ApJ, 492, L103
- Piro, L., et al. 1998, A&A, 331, L41
- Perley, D. A., et al. 2008, ApJ, 688, 470
- Perna, R., Armitage, P. J. & Zhang, B. 2006, ApJ, 636, L29
- Proga, D. & Zhang, B. 2005, MNRAS, 370, L61
- Racusin, J. L., et al. 2008, Nature, 455, 183
- Romano, P., et al. 2006, A&A, 450, 59
- Rykoff, E. S., et al. 2004, ApJ, 601, 1013
- Rykoff, E. S., et al. 2009, ApJ, 702, 489
- Sakamoto, T. et al. 2008, ApJS, 175, 179
- Sagar, R., et al. 2000, BASI, 28, 499
- Shaviv, N. J. & Dar, A. 1995, ApJ, 447, 863
- Vestrand, W. T., et al. 2006, Nature, 442, 172
- Wozniak, P. R., et al. 2006, ApJ, 642, L99
- Wozniak, P. R., et al. 2009, ApJ, 691, 495
- Zhang, B. B., Liang, E. W. & Zhang, B. 2007, ApJ, 666, 1002

Table 1. The AG parameters used in the CB model description of the smooth X-ray AG of Swift GRBs with superimposed flares. The CB model spectral index obtained from the temporal shape of the AG and that inferred from the measured XRT spectrum as reported in the Swift lightcurve repository (Evans et al. 2009) are compared in the last two columns.

GRB/SHB	t_b [s]	$\gamma_0 \theta$	$\beta_X = p/2$	$\beta_X = \Gamma_{Swift} - 1$
GRB050502B	674	0.73	0.96	0.945 (+0.077, -0.100)
SHB050724				0.81 (+0.14, -0.17)
GRB050820A	9545	1.19	1.10	0.966 (+0.051, -0.050)
GRB050916	2178	0.74	0.90	
GRB060206	9402	1.04	1.12	1.21 (+0.27, -0.24)
GRB060418	123	1.73	1.05	0.96 (+0.15, -0.14)
GRB060526	4828	1.35	1.02	0.931 (+0.086, -0.084)
GRB060729	32665	2.52	1.10	1.067 (+0.038, -0.037)
GRB060929	5383	1.27	0.91	1.22 (+0.25, -0.25)
GRB061007	40	0.15	1.08	1.018 (+0.087, -0.083)
GRB070704	5183	1.27	0.90	0.98 (+0.18, -0.33)
GRB071003	1214	1.94	1.08	0.984 (+0.107, -0.059)
XRF071031	5451	2.56	0.74	0.86 (+0.14, -0.15)
GRB080319B	86	0.14	1.08	1.03 (+0.064, -0.063)
XRF080330	541	4.61	0.89	0.89 (+0.13, -0.12)
GRB080506	7801	1.76	0.91	0.990 (+0.122, -0.077)
GRB080607	2904	0.53	0.91	1.102 (+0.098, -0.092)
GRB080810	3452	0.63	1.25	1.156 (+0.099, -0.089)
GRB080906	5790	0.90	0.96	1.049 (+0.069, -0.164)
GRB081102	1891	0.47	0.92	0.921 (+0.079, -0.114)
GRB081203A	436	0.91	1.15	1.096 (+0.089, -0.081)
GRB090102	348	0.80	0.95	0.858 (+0.078, -0.076)
GRB090417B	1259	0.63	1.04	1.09 (+0.11, -0.11)
GRB090618	1540	1.10	1.04	1.008 (+0.047, -0.046)
GRB090621A	1309	0.83	0.94	1.01 (+0.18, -0.18)
GRB090709A	1098	0.51	1.08	1.081(+0.076, -0.074)
GRB090812	598	1.34	0.92	0.914 (+0.138, -0.089)
GRB091029	5753	2.32	1.01	1.197 (+0.077, -0.070)

Table 2. The parameters of the ICFs and SRFs used in the CB model description of X-ray lightcurves of Swift GRBs. Values of parameters that are not well determined by a best fit are inserted within parentheses

GRB/SHB	flares	t_0 [s]	Δt [s]	$E_p[keV]/a[s]$	t_0 [s]	Δt [s]	$E_p[keV]/a[s]$
GRB050502B	ICF,SRF,	485.7	308.3	0.27 keV	13750	28950	6013 s
	SRF	58950	18911	3350 s			
GRB060418	ICF,ICF	60	12	0.13keV	9.9	118	0.13keV
GRB060206	SRF,SRF	1.19	32.2	235 s	653	3427	3645 s
	SRF	609359	245909	1980979 s			
SHB050724	ICF,ICF	1.58	114	1.08 keV	469	1422	1.32 keV
	ICF	9757	49512	3.53 keV			
GRB050916	SRF,ICF				17836	1335	91 keV
	ICF	9757	49512	3.53 keV			
GRB050916	SRF,ICF				17836	1335	91 keV
GRB060526	SRF,ICF				233	42.5	0.15 keV
	ICF,SRF	280	25.7	60.2 keV			
GRB060929	SRF,ICF				472	45	117 keV
GRB071031	ICF,ICF	84.8	46.2	13.2 keV	131	33.8	0.74 keV
	ICF,ICF	181.7	30.5	4.3 keV			
	ICF,ICF	328	176	2.74 keV			
	ICF	4351	1201	4.5 keV			
	SRF,SRF	16743	5463	4.2 s			
GRB070704	SRF,ICF	(63)	(0.35)	(25 s)	472	45.22	117 keV
GRB080506	ICF,SRF	130	36.7	14.4 keV	211	43	171 s
	ICF,ICF	433	(41)	(159 keV)			
GRB080607	ICS,ICF	65.9	8.6	145 keV	113.9	(15.4)	(350 keV)
	SRF,SRF	222	332	0.6 s			
GRB081203A	SRF	79	10.8	(0)			
GRB080810	ICF,SRF,	74	16	25.5 keV	98.6	4.6	34 s
	ICF,SRF	196	(14)	(203 keV)			
GRB080906	SRF,SRF,	(49)	(1)	(47.7 s)	157	27.5	10.75 s
	SRF,ICF	490	8.58	200 s			
GRB081102	SRF,ICF	63	11	42.7 s	914	88	111 keV
GRB090417B	SRF,ICF	336.2	203	82.6 s	1227.8	431	1.96 keV
GRB090618	ICF,SRF	65.9	12.9		(0)	884	(0)

Table 2—Continued

GRB/SHB	flares	t_0 [s]	Δt [s]	$E_p[keV]/a[s]$	t_0 [s]	Δt [s]	$E_p[keV]/a[s]$
GRB090621A	SRF,ICF	150.6	2.6 s	215	217.9	50.4	0.95 keV
GRB090709A	ICF,SRF,	70.3	20.61	2.38 keV	75.5	14.3	116 s
	SRF,ICF	165.8	110.2	149	324.6	37	187 s
GRB091029	ICF,ICF	0	38.8	9.8 keV	218.6	102.5	10.9 keV
	SRF	209360	245909				

Table 3. The parameters of the CB model description of the early-time optical SRFs/peaks in GRBs 080319B, 060206, 071003, 071031 and 080330

Flare	t_0 [s]	a [s]	t_{exp} [s]	β_O
GRB 080319B:				
SRF1	9.50	3.52	10.24	0.70
SRF2	32.37	3.52	5.83	0.70
SRF3	39.54	3.52	6.96	0.70
GRB 060206:				
SRF1	~ 0	548	$\ll a$	0.50
SRF2	2526	1214	887	0.80
SRF3	4286	3113	31	0.87
GRB 071003:				
SRF1	4.11	$\ll t_{exp}$	16.7	0.79
SRF2	125	139	14.6	1.03
SRF3	441	348	$\gg a$	0.75
GRB 071031:				
SRF1	90	97	1875	0.62
SRF2	540	$\ll t_{exp}$	43	0.63
SRF3	2335	7900	158	0.63
SRF4	10318	13372	134	0.63
GRB 080330:				
SRF1	0.29	32	946	0.67
SRF2	3.40	1716	235	0.67
SRF3	3416	1491	18337	0.67

Table 4. CB model parameters of the ICS γ peaks in GRB 990123

Peak	t_0 [s]	Dt [s]	E_p [keV]	A [counts s $^{-1}$]
1	-5.57	15.4	300	4.00×10^3
2	19.42	4.28	1450	3.95×10^4
3	29.88	0.87	500	6.74×10^3
4	32.95	5.43	800	2.75×10^4
5	43.67	4.99	500	1.11×10^4
6	52.77	4.30	450	1.05×10^4
7	61.09	4.10	450	1.21×10^4
8	70.35	5.63	600	1.69×10^4
9	85.50	1.86	200	6.64×10^3

Table 5. The parameters used in the CB model description of unresolved prompt emission SRF in the optical lightcurves of Swift GRBs.

GRB	flare	t_0 [s]	a [s]	t_{exp} [s]	β
GRB990123	SRF	22	$\lesssim 10$	1.67	0.50
GRB030418	SRF	200	4097	$\ll a$	0.56
GRB050820A	SRF	109	479	$\ll a$	
GRB061007	SRF	15.8	90.37	$\ll a$	0.60
GRB081203A	SRF	0	316	368	0.90
GRB090102	SRF	1.65	0.13	2.16	0.53
GRB090618	SRF	118	~ 0	61	0.51

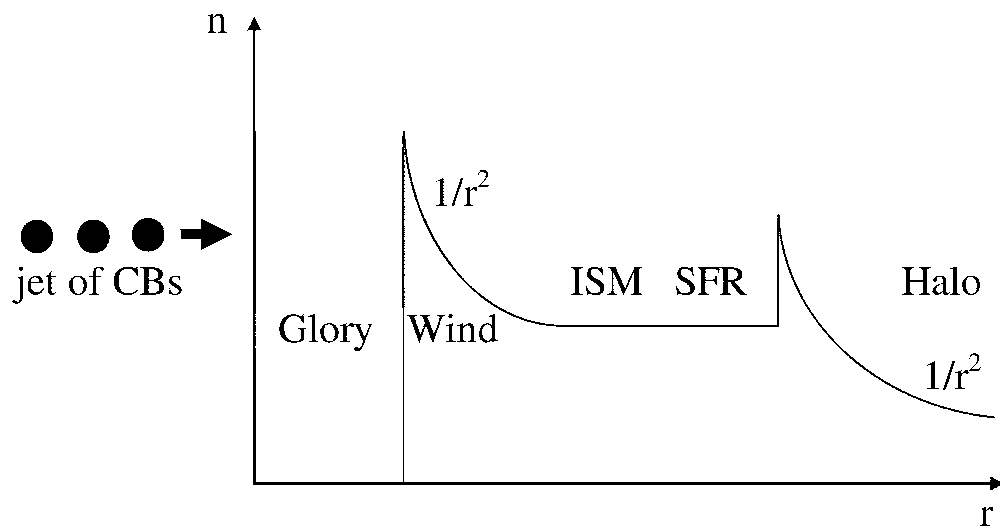


Fig. 1.— Schematic illustration, not in scale, of the typical environment encountered by a highly relativistic jet ejected in core collapse SN that escapes from the star formation region into the galactic halo.

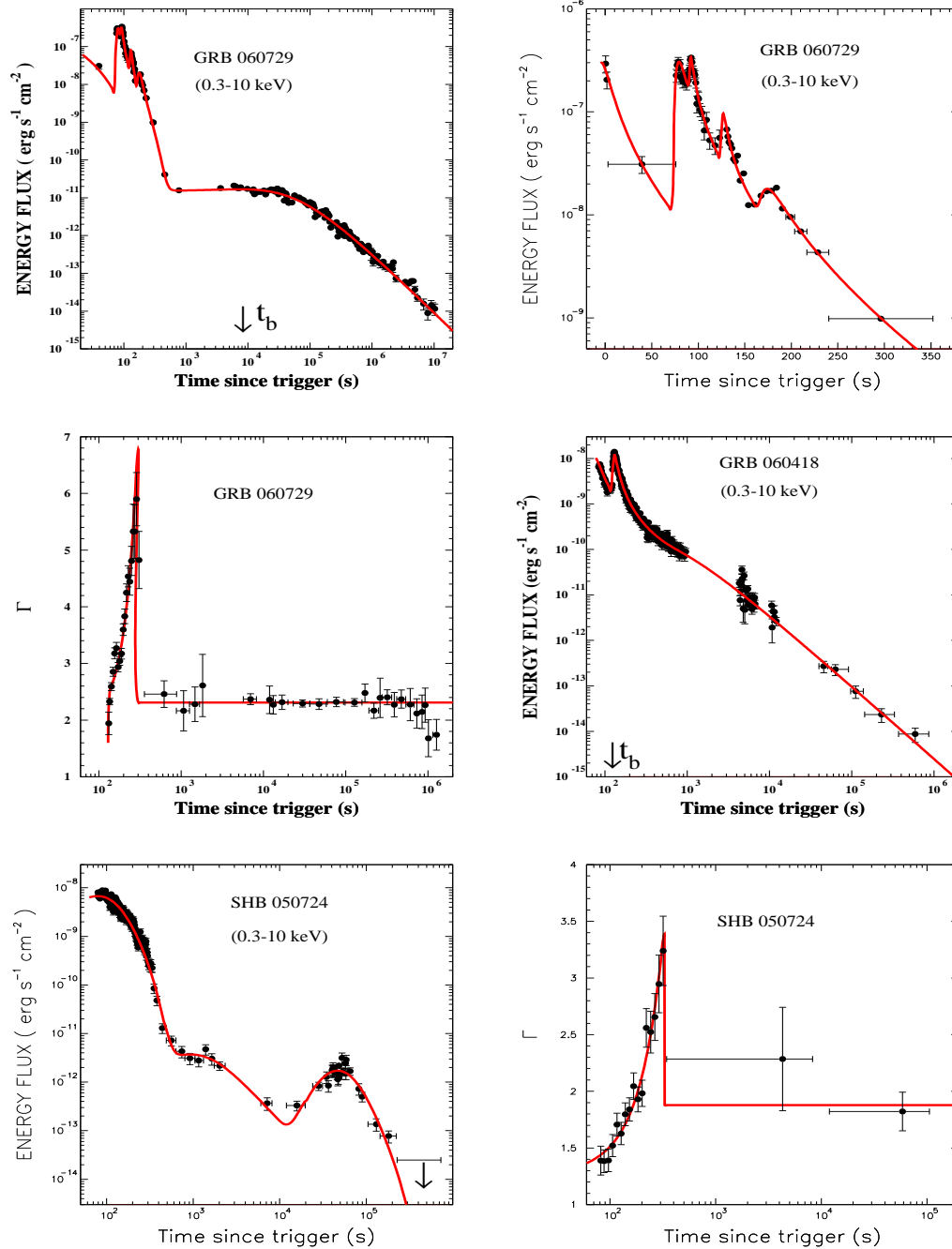


Fig. 2.— Comparison between 0.3-10 keV lightcurves of Swift GRBs (Swift/XRT lightcurve repository (Evans et al. 2009)) with early-time X-ray flares and their CB model description with the parameters listed in Table 1. **Top left (a):** Comparison between the Swift ‘canonical X-ray lightcurve’ (Nousek et al. 2006) of GRB 060729 and its CB model description. **Top right (b):** Zoom on the prompt emission and fast decay phase in a. The CB model lightcurve of the prompt emission consists of a sum of 5 ICFs. **Middle left (c):** Comparison between the evolution of the effective photon spectral index of GRB 060729 in the 0.3-10 keV X-ray band as inferred from the Swift XRT observations by Zhang et al. (2007) and that inferred from the CB model lightcurve. **Middle right (d):** Comparison between the non-canonical X-ray lightcurve of GRB 060418 and its CB model description. **Bottom left (e):** Comparison between the XRT and CB model lightcurves of SHB 050724. **Bottom right (f):** Comparison between the evolution of the effective photon spectral index in the 0.3-10 keV X-ray band as inferred by Zhang et al. (2007) from the observations of SHB 050724 with the Swift XRT and that inferred from the CB model lightcurve.

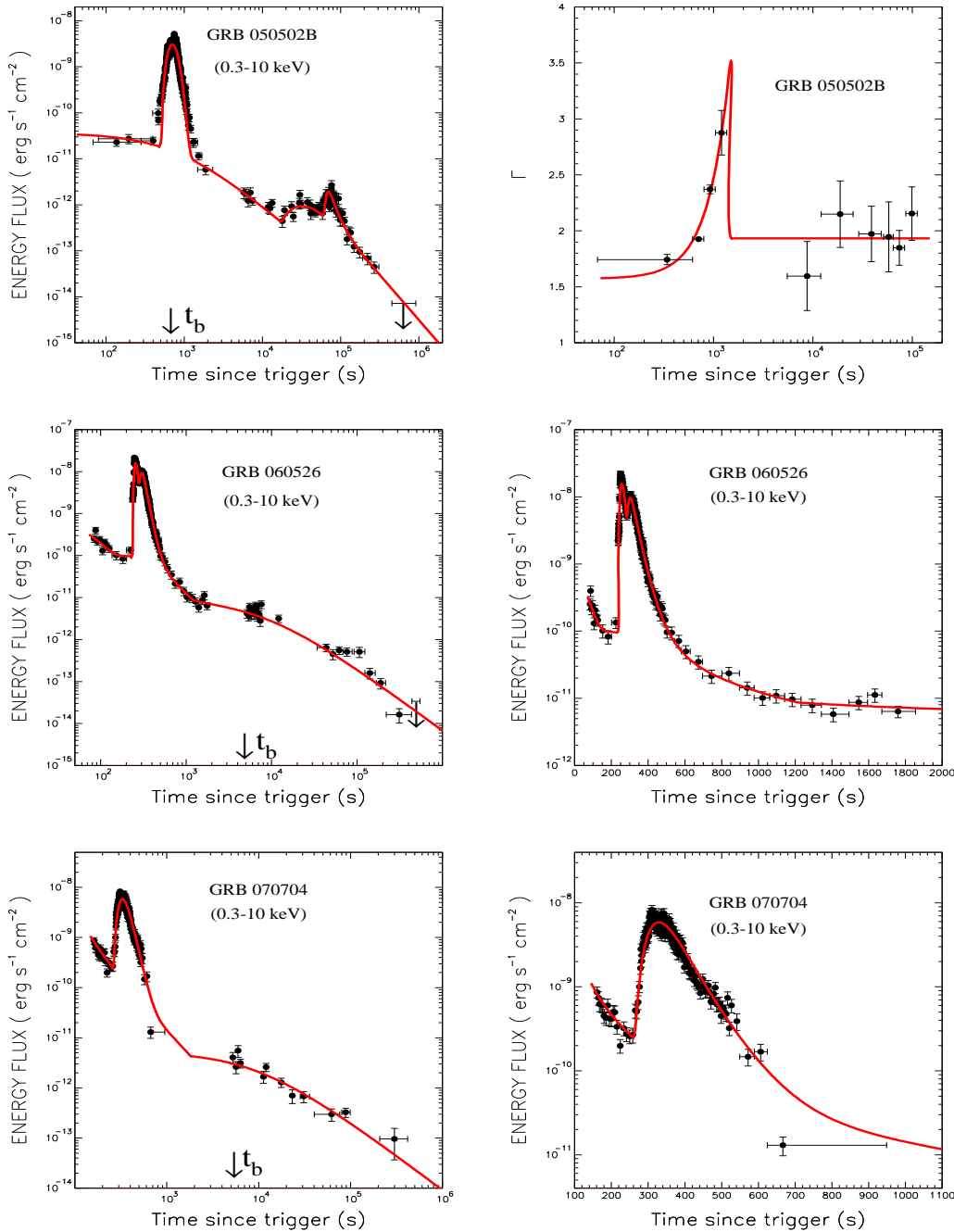


Fig. 3.— Comparison between the 0.3-10 KeV X-ray lightcurves of GRBs with prominent flares in their X-ray afterglow that were measured by the Swift XRT and reported in the Swift/XRT lightcurve repository http://www.swift.ac.uk/xrt_curves/ (Evans et al. 2009) and their CB model description with the parameters listed in Table 1. **Top left (a):** GRB 050502B. **Top right (b):** Comparison between the evolution of the effective photon spectral index of GRB 050502B in the 0.3-10 keV X-ray band as inferred by (Zhang et al. 2007) from the Swift XRT observations and that inferred from the CB model lightcurve. Note the similarity between this Fig. and Figs. 2c,f. **Middle left (c):** GRB 060526. **Middle right (d):** Zoom on the prominent X-ray flare in the early-time AG of GRB 060526. **Bottom left (e):** GRB 070704. **Bottom right (f):** Zoom on the prominent X-ray flare in the early-time AG of GRB 070704.

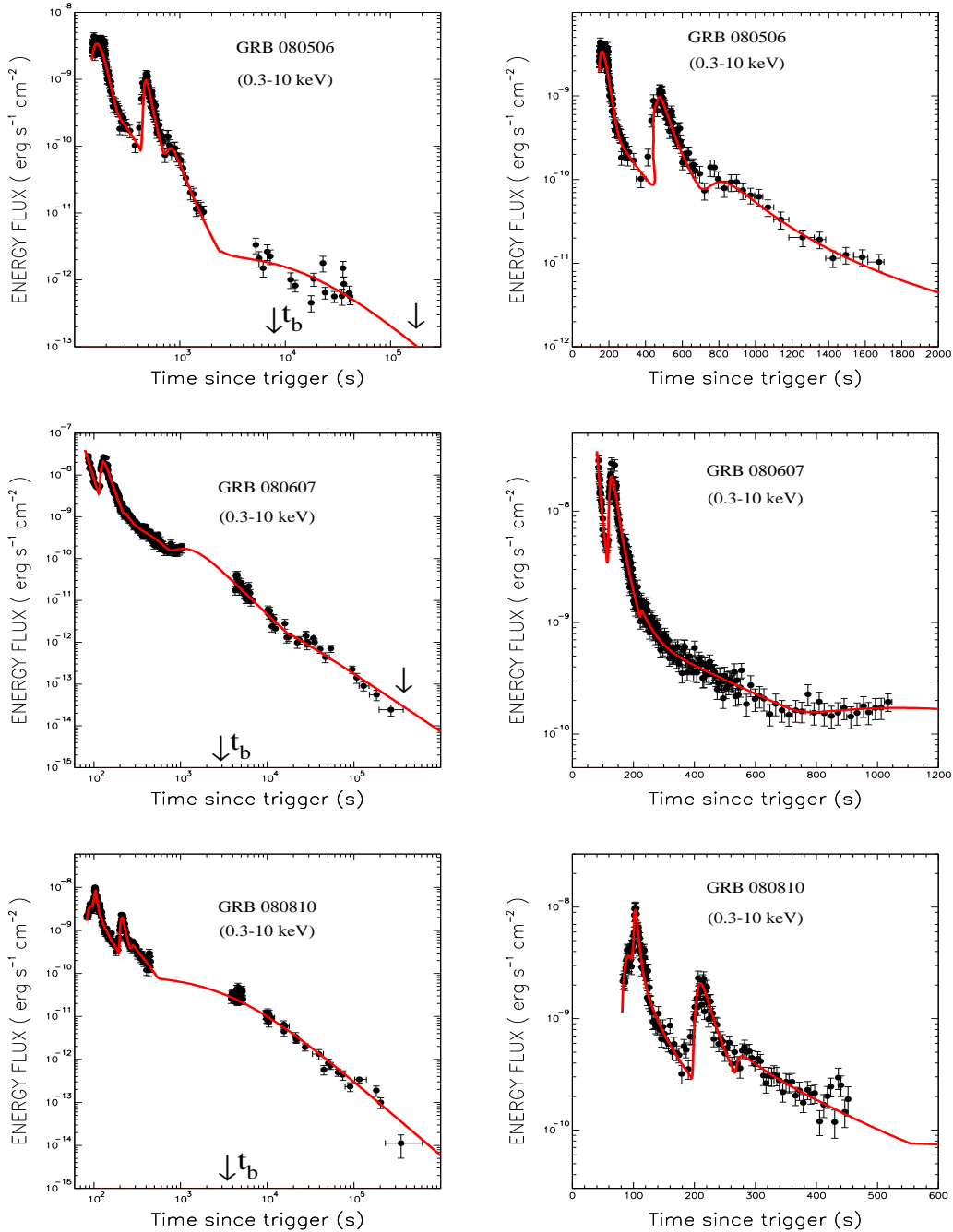


Fig. 4.— Comparison between the 0.3-10 KeV X-ray lightcurves of GRBs with prominent flares in their X-ray afterglow that were measured by the Swift XRT and reported in the Swift/XRT lightcurve repository http://www.swift.ac.uk/xrt_curves/ (Evans et al. 2009) and their CB model description with the parameters listed in Table 1. **Top left (a):** GRB 080506. **Top right (b):** Zoom on the prominent X-ray flare in the early-time AG of GRB 080506. **Middle left (c):** GRB 080607. **Middle right (d):** Zoom on the prominent X-ray flare in the early-time AG of GRB 080607. **Bottom left (e):** GRB 080810. **Bottom right (f):** Zoom on the prominent X-ray flare in the early-time AG of GRB 080810.

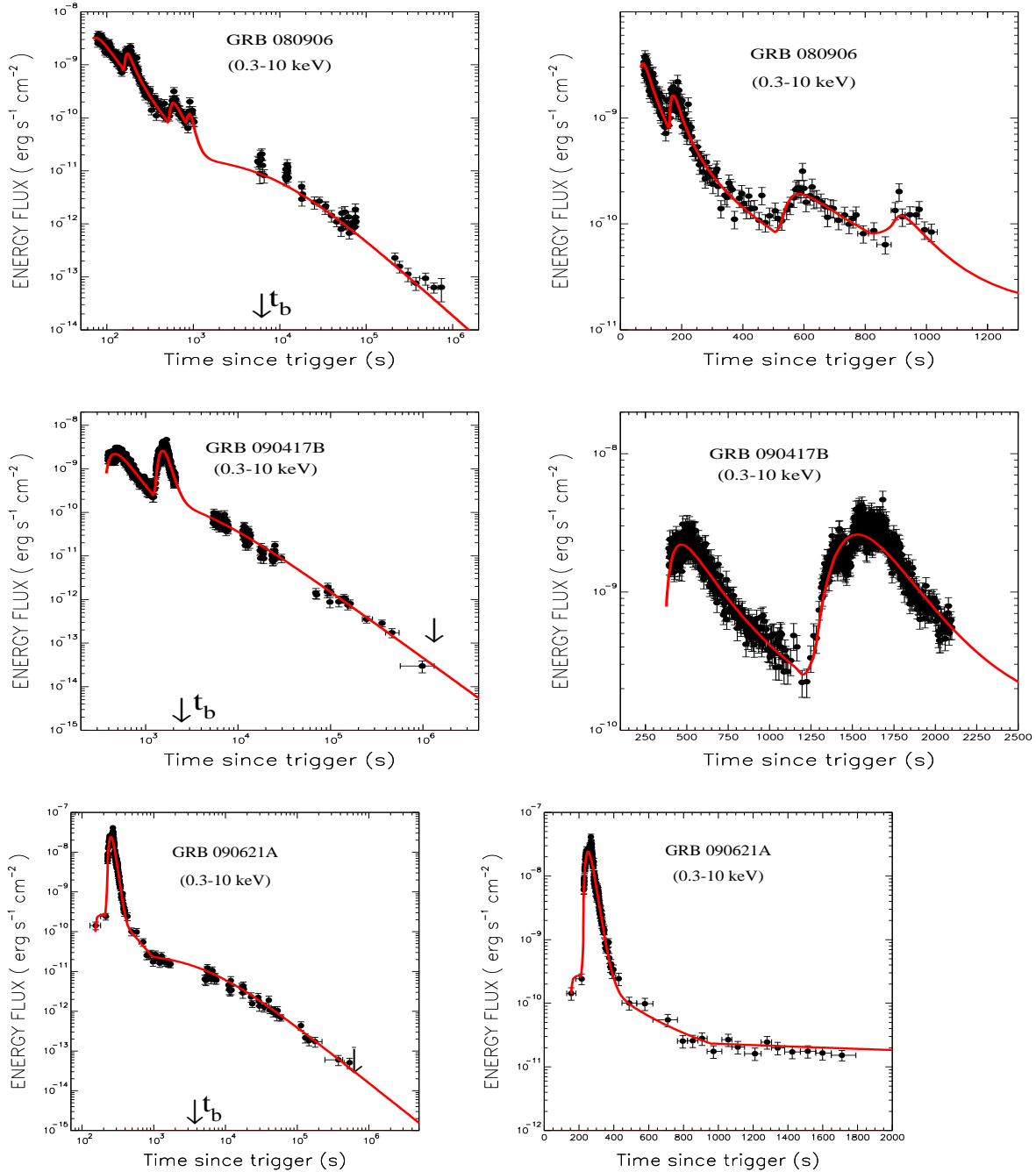


Fig. 5.— Comparison between the 0.3-10 KeV X-ray lightcurves of GRBs with prominent flares in their X-ray afterglow that were measured by the Swift XRT and reported in the Swift/XRT lightcurve repository (Evans et al. 2009) and their CB model description with the parameters listed in Table 1. **Top left (a):** GRB 080906. **Top right (b):** Zoom on the prominent X-ray flare in the early-time AG of GRB 080906. **Middle left (c):** GRB 090417B. **Middle right (d):** Zoom on the prominent X-ray flare in the early-time AG of GRB 090417B. **Bottom left (e):** GRB 090621A. **Bottom right (f):** Zoom on the prominent X-ray flare in the early-time AG of GRB 090621A.

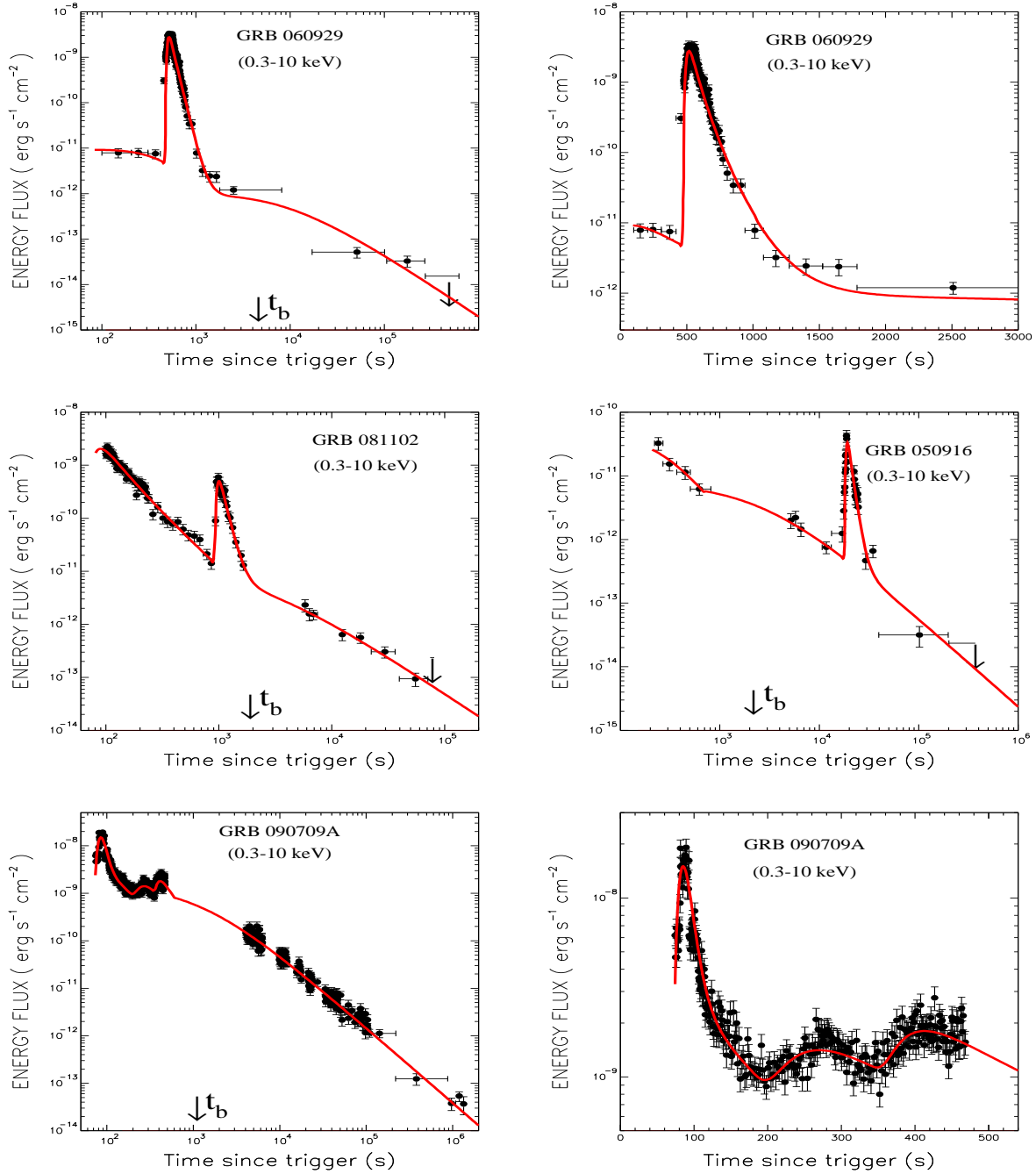


Fig. 6.— Comparison between the 0.3-10 KeV X-ray lightcurves of GRBs with prominent flares in their X-ray afterglow that were measured by the Swift XRT and reported in the Swift/XRT lightcurve repository (Evans et al. 2009) and their CB model description with the parameters listed in Table 1. **Top left (a):** GRB 060929. **Top right (b):** Zoom on the flare in the AG of GRB 060929. **Middle left (c):** GRB 081102. **Middle right (d):** GRB 050916. **Bottom left (e):** GRB 090709A. **Bottom right (f):** Zoom on the early-time X-ray flares in the AG of GRB 090709A.

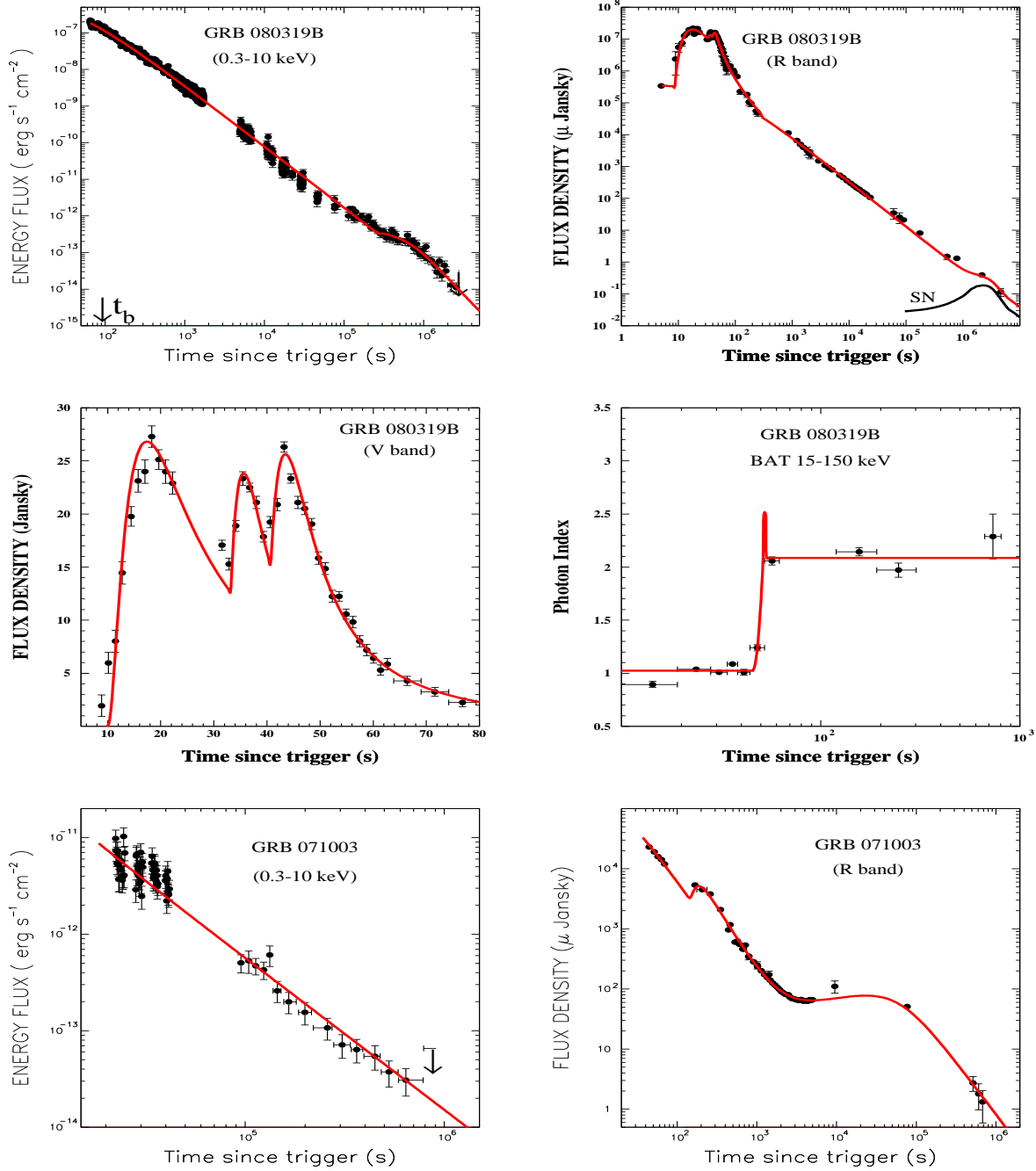


Fig. 7.— Comparison between the observed early-time X-ray and optical lightcurves of very bright GRBs and their CB model descriptions. GRB 080319B - **Top left (a)**: 0.3-10 keV XRT lightcurve. **Top right (b)**: R-band lightcurve. **Middle left (c)**: The early-time optical flares. **Middle right (d)**: The spectral index lightcurve. GRB 071003 - **Bottom left (e)**: The 0.3-10 keV XRT lightcurve. **Bottom right (f)**: The entire R-band lightcurve.

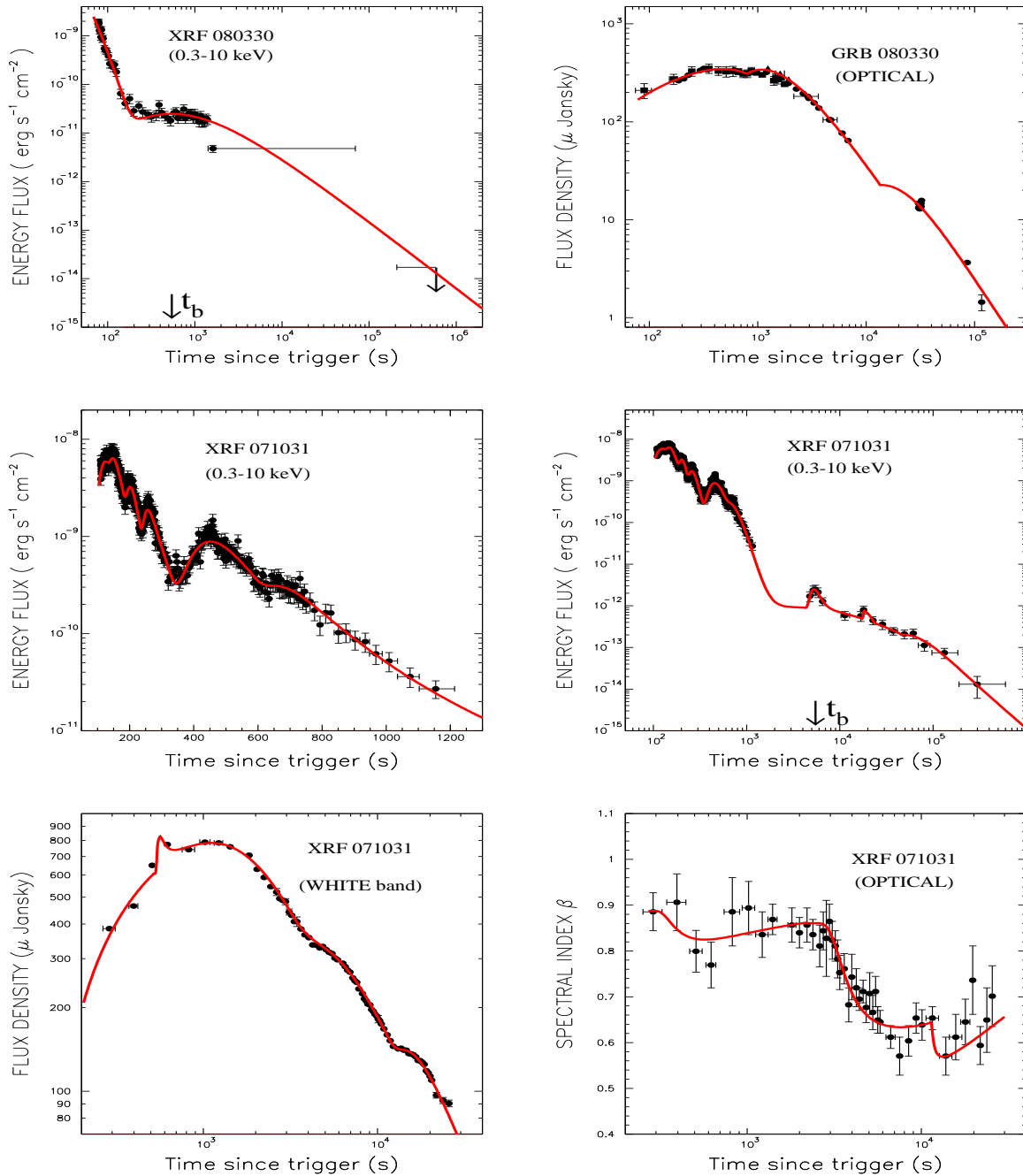


Fig. 8.— Comparison between the observed early-time X-ray and optical lightcurves of XRFs and their CB model description. Unlike the X-ray flares, the early-time optical flares are barely resolvable to separate optical flares. XRF 080330 - **Top left (a)**: The 0.3-10 keV XRT lightcurve. **Top right (b)**: The optical (white) lightcurve. XRF 071031- **Middle left (c)**: The 0.3-10 keV XRT lightcurve. **Middle right (d)**: Zoom on the early time XRT lightcurve. **Bottom left (e)**: The early-time optical (white) lightcurve. **Bottom right (f)**: Evolution of the optical spectral index.

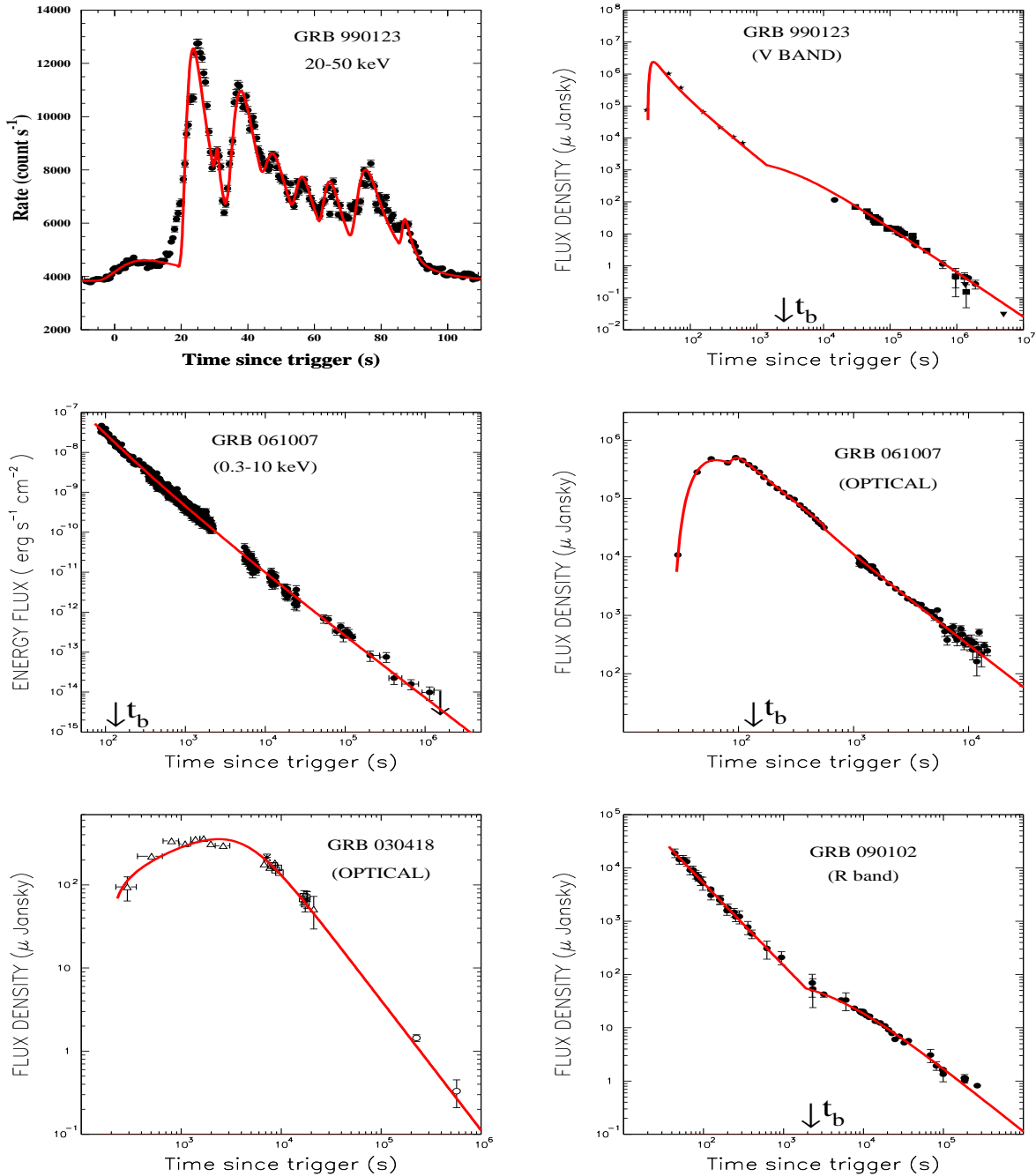


Fig. 9.— Comparison between observed and CB model description of lightcurves. GRB 990123 - **Top left (a)**: Comparison between the 20-50 keV BATSE lightcurve (Briggs et al. 1999) and its CB model description, Eq. (1), in terms of 9 ICS peaks + a constant background of 3850 counts s⁻¹. **Top right (b)**: Comparison between the V band lightcurve of GRB 990123 and its CB model description assuming a single CB moving in circumstellar density profile $\propto 1/r^2$ overtaken by a constant ISM density around an observer time $t=1000$ s. The prompt flare was not resolved into separate flares. GRB 061007 - **Middle left (c)**: The 0.3-10 keV XRT lightcurve. **Middle right (d)**: The optical lightcurve with evidence for at least two early time overlapping flares. **Bottom left (e)**: The optical (white) lightcurve of GRB 030418 - **Bottom right (f)**: The R-band lightcurve of GRB 090102 with evidence for a tail of a prompt optical flare.

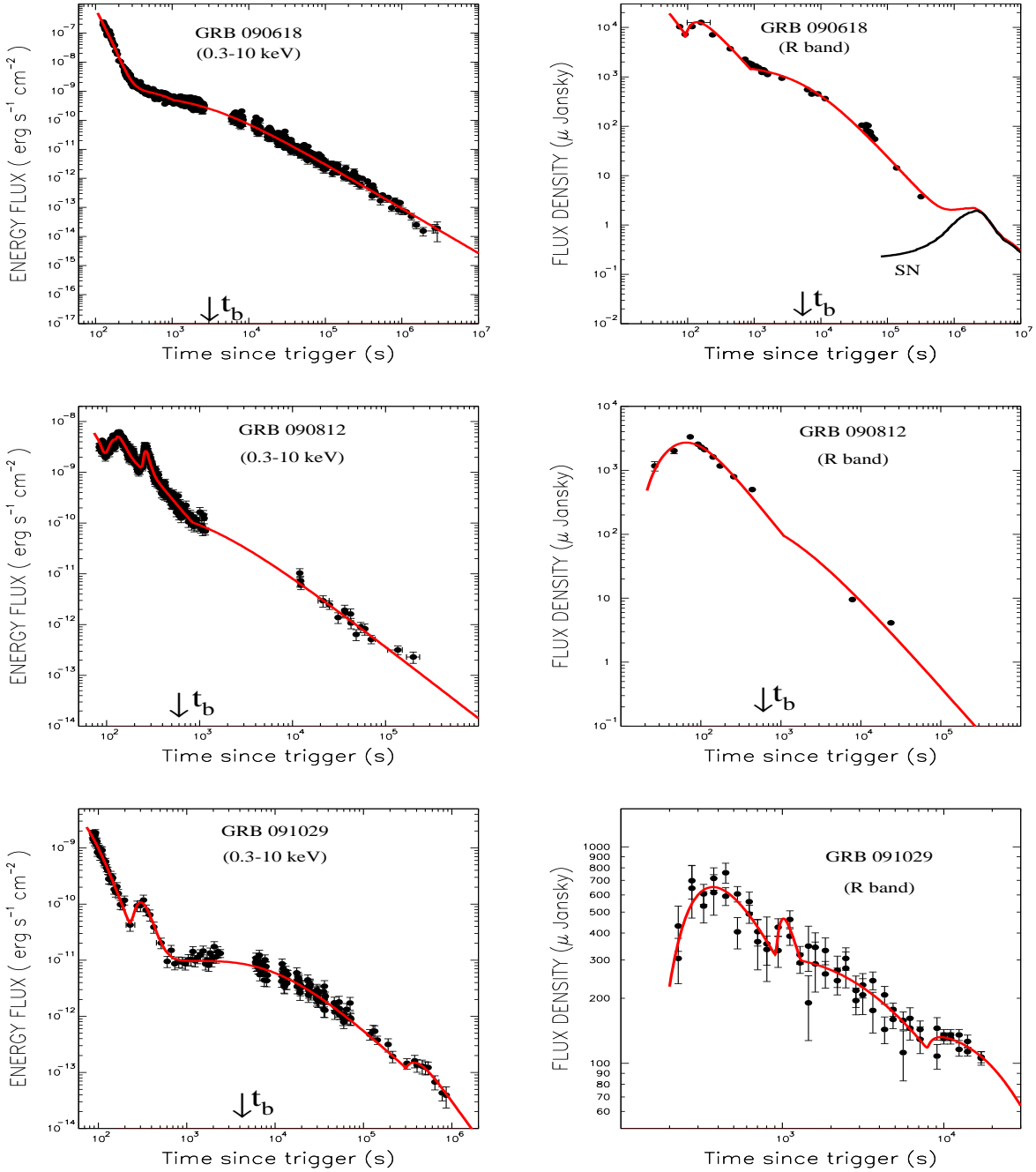


Fig. 10.— Comparison between the observed early-time X-ray and optical lightcurve of GRBs and their CB model description. The X-ray and optical emissions do not appear to be correlated. GRB 090618 - **Top left (a)**: The 0.3-10 keV lightcurve. **Top right (b)**: The optical R-band lightcurve. GRB 090812 - **Middle left (c)**: The 0.3-10 keV XRT lightcurve. **Middle right (d)**: The optical R-band lightcurve with evidence for at least two early time overlapping flares. GRB 091029 - **Bottom left (e)**: The 0.3-10 keV X-ray lightcurve. **Bottom right (f)**: The R-band lightcurve with possible evidence for unresolved optical flares.

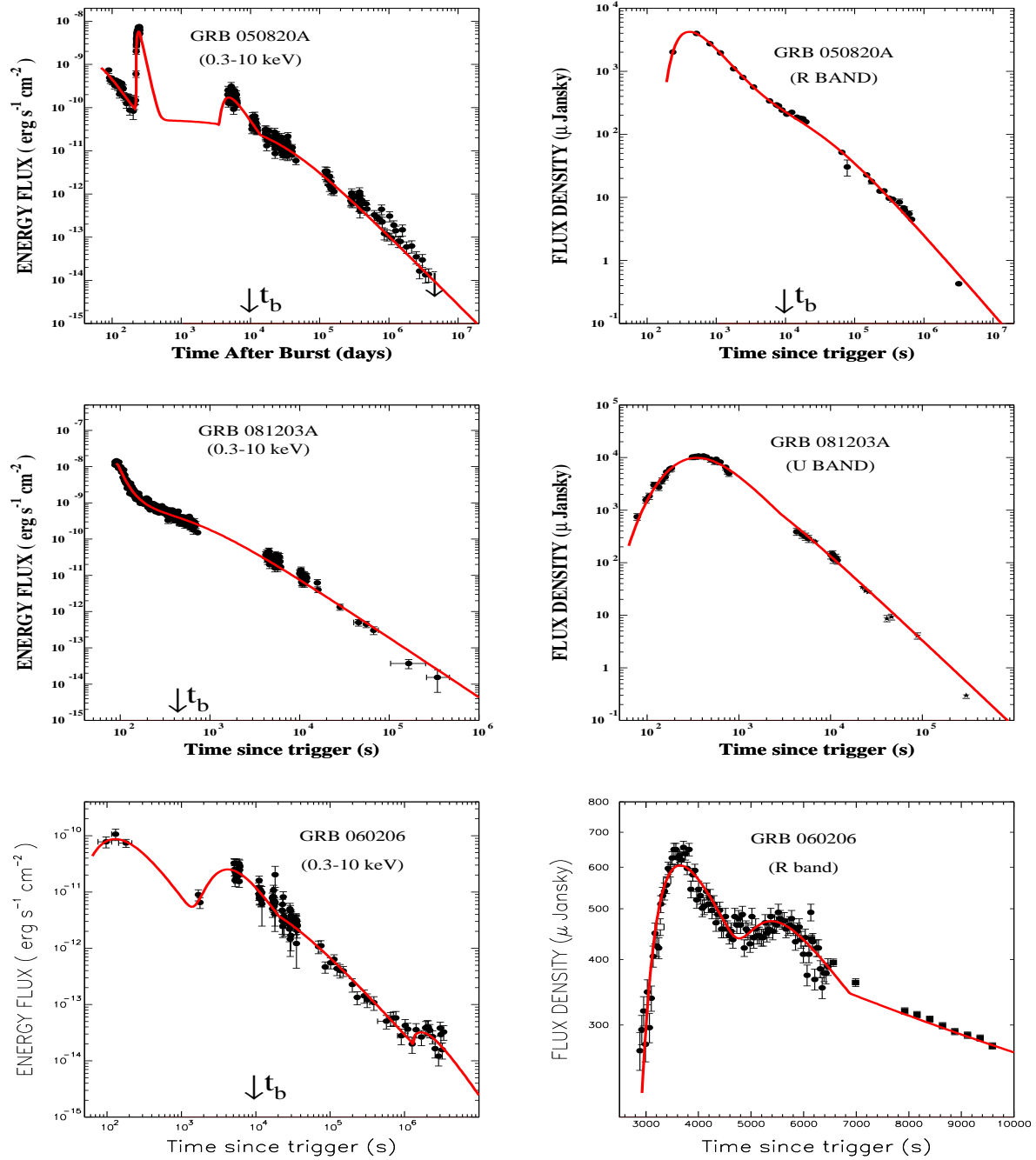


Fig. 11.— Comparison between the observed X-ray and optical lightcurves of XRFs and their CB model description. The early-time optical lightcurves are approximated by a single (unresolved) SRF. GRB 050820A - **Top left (a)**: The 0.3-10 keV XRT lightcurve. **Top right (b)**: The optical R-band lightcurve. GRB 081203A **Middle left (c)**: The 0.3-10 keV XRT lightcurve. **Middle right (d)**: The optical U-band lightcurve. GRB 060206 **Bottom left (e)**: The 0.3-10 keV lightcurve with poorly resolved late-time flares. **Bottom right (f)**: The R-band lightcurve with well resolved late-time SRFs.